17. MINERALOGY AND GEOCHEMISTRY OF SEDIMENTARY DEPOSITS ON EMPEROR SEAMOUNTS, SITES 430, 431, AND 432: AUTHIGENESIS OF SILICATES, PHOSPHATES AND FERROMANGANESE OXIDES

Anne Marie Karpoff, Irène Peterschmitt, and Michel Hoffert, Centre de Sédimentologie et Géochimie de la Surface (C.N.R.S.) and Institut de Minéralogie, Strasbourg, France

INTRODUCTION

One of the objectives of Leg 55 was to investigate the Tertiary history of sedimentation and environment on the Emperor Seamounts after their volcanic activity. For the three first sites, 430, 431, and 432, drilled on Ōjin, Nintoku, and Yōmei Seamounts, the Neogene sedimentary deposits are not well represented and are not typical pelagic sediments. Except for two holes (430A and 432), where we found calcareous oozes, the sediments are heterogeneous sands, gravels, and pebbly mudstones with a wide range in grain size and composition. Two phenomena characterize these deposits: the inheritance of volcaniclastic material and its alteration, and the authigenesis of secondary minerals including silicates, phosphates, and ferromanganese oxides formed under volcanic influence in a marine environment.

The three first sites are located in the central part of the Emperor Chain (Figure 1) at Ōjin (37°59 'N, 170°35 'E), Nintoku (41°20 'N, 170°22 'E), and Yōmei (42°25 'N, 170°22 'E) seamounts. The six holes studied appear to be in a lagoonal depression, the top of a reef flat, and a faulted terrace, respectively (Greene et al., this volume). The lithologic composition of the cored formations described in the site reports is summarized in Figure 2, which also shows the positions of the samples studied. The ages of the deposits are established by Koizumi, Takayama, Ling, and Butt (this volume). Because of the heterogeneity of the sediments, the sampling was very discontinuous. The objectives of this study are to establish the nature of the different components from the sedimentary deposits and to examine their evolution and relationships.

LITHOLOGY AND MINERALOGY OF SEDIMENTARY DEPOSITS FROM SITES 430, 432, AND 431

Methods

The mineralogical composition of the sediments was determined using X-ray diffraction techniques. The X-ray diffraction charts from non-oriented powders have been obtained using bulk material, which was not always the whole sedimentary deposit, under the following conditions: CuKα radiation, Ni filter, 98 kV/18 mA, 0.1°–1° slits, 1°/min. speed. For some samples, the identification of clay minerals in the <2 μm and <63 μm fractions was made on three types of oriented aggregates: untreated, ethylene-glycol-treated, and heated,

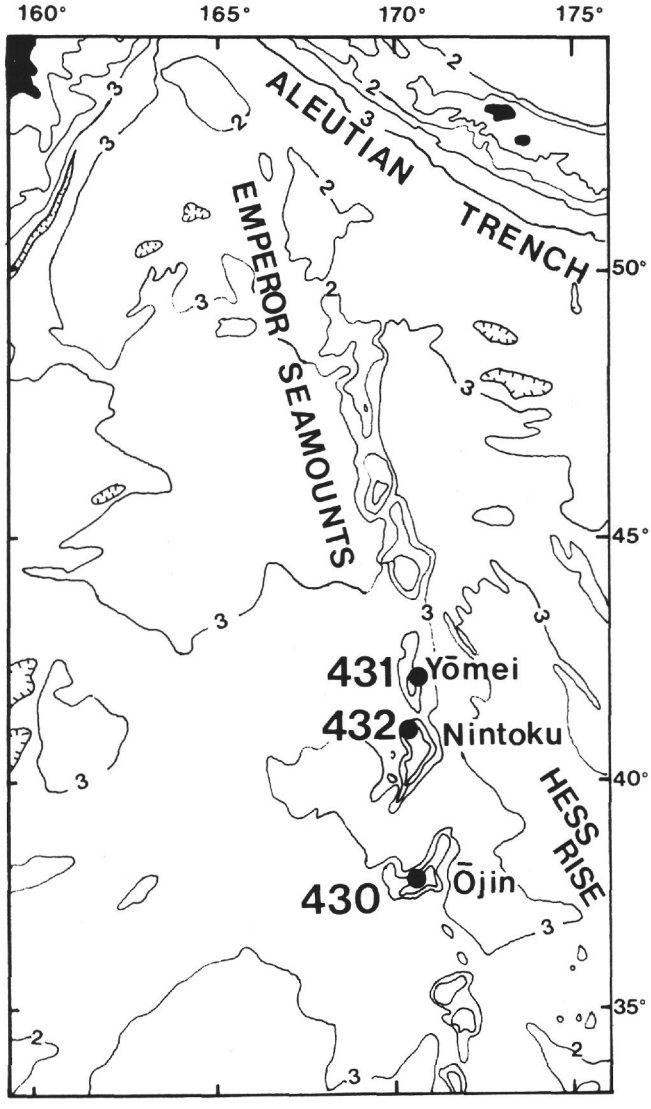

Figure 1. *Map of western North Pacific, showing Emperor Seamounts and locations of Sites 430, 431, and 432. Depths to the ocean floor are shown in units of 1000 fathoms.*

according to the methods of the Institut de Géologie in Strasbourg (Mise au point collective, 1975).

Some clay fractions were also studied by microdiffraction on isolated particles, by transmission electron microscope (TEM, Phillips EM 300) using the method of Trauth et al. (1977). The morphology of special sam-

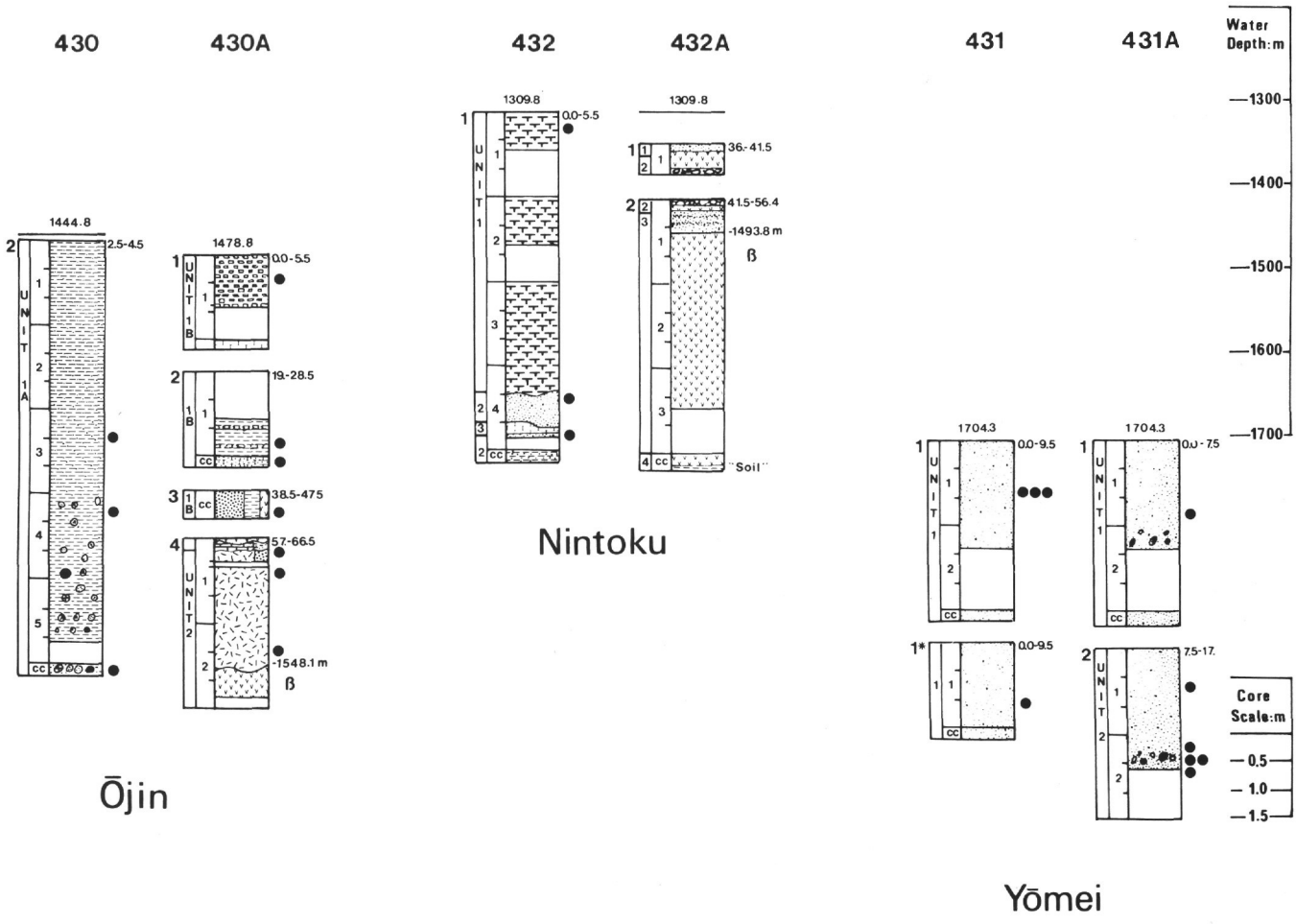

Figure 2. *Schematic description of cores drilled into the Ōjin, Nintoku, and Yōmei seamounts.* ●*:Position of samples studied from Sites 430, 431, and 432. The scale of water depth differs from the core-depth scale.*

ples was observed by scanning electron microscope (SEM, Cameca 07).

Results

Lithologic facies descriptions of the samples and their mineralogical compositions are presented in Table 1 for Sites 430, 432, and 431, in geographic order from the south to the north.

Site 430, Ōjin Seamount

The sedimentary sequence at Hole 430 is composed of a very disturbed pebbly mudstone (Unit 430-IA) containing a variety of clasts, including volcanic gravels and ferromanganese crust fragments or small nodules. Calcite, plagioclase, and iron–manganese oxihydroxides occur in these deposits. The clays are smectites, illite, and chlorite. In the core-catcher sample from Core 2, the specimen studied is a small nodule, two centimeters in diameter, with a nucleus composed of feldspar and trace amounts of clays and zeolites; the cortex of the nodule is made up of iron–manganese oxihydroxide layers.

In Hole 430A, the upper sedimentary deposits are calcareous ooze, sand, and calcareous sandstone (Unit 430-IB), which contain volcanic fragments or basalt pebbles. Carbonate-apatite occurs associated with calcite in the upper part of this unit. McKenzie et al. (this volume) describe the occurrence of zeolites in the lower calcareous formation.

The underlying sequence (Unit 430-II) is a black volcanic ash with interlayered fine calcareous material. Volcanic glass and clays are abundant, and small amounts of plagioclase and zeolite are also present. The clays are smectites and appear to be saponite.

Site 432, Nintoku Seamount

The sediments from the top of Hole 432, foraminifer ooze (Unit 432-I) and fine-grained sand (Unit 432-II), contain calcite, plagioclase, kaolinite, smectite, and trace amounts of quartz.

The well-consolidated calcite-cemented sandstone at Hole 432A is not studied here. Deposited in shallow water, this sandstone appears to be a lagoonal and reef deposit showing no volcanic influences.

Site 431, Yōmei Seamount

The two lithologic units from Site 431 differ from one another more in color and grain-size heterogeneity than in mineralogical composition.

In Hole 431 and the top of Hole 431A (Unit 431-I), the black ferromanganese sand contains a variety of

TABLE 1
Lithologic Description and Mineralogical Data for Samples from Sites 430, 431, and 432

Sample (Interval in cm)	Lithology	Sample Description	Bulk Sample Major Constituent	<2μm Fraction Major Constituent
430-2-3, 43-52	Unit IA – Watery muddy sand, very dark grayish brown: 10 YR 3/2	Total deposit with oxide fragments	Calc. Plag. Fe-Mn ox. Ap. Mn = ox.	Chl. Int.
2-4, 20-25	Unit IA – Pebbly mud, unconsolidated clastic gravel, dark brown: 10 YR 3/3	Total deposit	Calc. Plag. Fe-ox. Tr Ap. Zeo. Clays	Sm.Ill.Tr Chl.
2,CC	Unit IA – Pebbly mud, clastic gravel: mudstone, nodules	Nodule: cortex of oxides only	Mn-oxide (Todorokite), Tr Zeo.	
430A-1-1, 45-49	Unit IB – Silty calcareous ooze, very pale brown: 10 YR 8/4	Total deposit	Calc. Ap.	
2-1, 127-129	Unit IB – Calcareous sand, very pale brown: 10 YR 7/3	Total deposit	Calc. Tr Ap. Tr Qu.	
2,CC	Unit IB – Limestone nodule and calcareous sand with volcanic fragments	Fragment of altered basalt	Plag. Fe-ox. Clays	
4-1, 10-16	Limit Units IB and II – calcareous sandstone, mud, and ash layer	Calcareous sandstone	Calc.	
4-1, 64-66	Unit II – Ash layer, dark gray: 5 Y 3/1 - 5 Y 2.5/1	Total deposit	Plag. Clays	Sm. °
4-2, 52-55	Unit II – Ash layer	Total deposit	Plag. Clays. Tr Zeo.	Sm. °
432-1-1, 30-34	Unit I – Foraminifer ooze, grayish brown: 2.5 Y 5/2	Bulk sample	Calc. Hal.	
1-4, 76-80	Unit II – Fine-grained sand, very dark grayish brown: 2.5 Y 3/2	Bulk sample	Calc. Qu. Clays	Kaol. Tr Sm.
1-4, 140-145	Unit II – Fine-grained sand	Bulk sample	Calc. Hal. Plag. Qu. Clays	
431-1-1, 80-87(a)	Unit I – Fe-Mn oxides gravel, black: 7.5 YR 2.5	Fe-Mn fragment	Mn-oxides (Tod)	
1-1, 80-87(b)		Pale yellow firm particles	Sm. Tr Zeo.	Sm.
1-1, 80-87(c)	Heterogeneous sand of crust fragments, compacted yellow particle of phosphates and authigenic silicates	Yellow particles with hard pale brown slab. Yellow firm particles	Ap. Sm.	
1*-1, 103-105			Ap. Sm.	
431A-1-1, 138-140	Unit I – Fe-Mn oxides, gravel and calcareous sand	Bulk sample	Calc. Ap. Qu. Mn-ox. Tr Clays	
2-1, 76-78	Unit II – Heterogeneous sand, olive brown: 2.5 Y 4/4, with olive yellow (2.5 Y 6/6), black and white particles	Olive yellow particles	Sm. Ap. Tr Plag. Mn-ox.	Sm.
2-2, 43-45	"	Oxide fragment	Tod.	
2-2, 45-47(a)	"	Fe-Mn crust fragment (oxides only)	Tod.	
2-2, 45-47(b)	"	Fe-Mn crust fragment (heterogeneous part)	Plag. Clays. Mn-ox.	
2-2, 52-54	"	Pale yellow particles	Sm. Tr Zeo.	

Notes: Calc.: calcite; Plag.: plagioclase (often anorthite); Fe-ox.: mixed hematite and geothite. Ap.: carbonate-apatite; Hal.: halite; Qu.: quartz; Mn-ox.: manganese oxide; Tod.: todorokite; Zeo.: zeolites; Sm.: smectites; Sm. °: Saponite; Chl.: chlorite; Ill.: illite; Kaol.: kaolinite; Int.: interstratified clays; Tr: traces.

volcanic pebbles and small amounts of yellow firm particles. Near the bottom of Hole 431A (Unit 431-II), the yellow particles are abundant in an olive-brown heterogeneous sand, and are associated with volcanic glass and volcaniclastic material.

The prevalent mineral assemblage of these units consists of black fragments of iron-manganese oxihydroxides and authigenic smectite, carbonate-apatite, and trace amounts of zeolite (phillipsite), which make up the yellow and yellowish brown firm aggregates. These authigenic components were investigated in detail.

OCCURRENCE OF TWO TYPES OF SMECTITES: PRIMARY SAPONITE AND AUTHIGENIC NONTRONITE

Olive-Gray Ash, Hole 430A

In the lower part of the sedimentary deposits from Hole 430A, a black to dark olive-gray volcaniclastic sand is interbedded with calcareous ooze and sandy mud. This ash is composed primarily of clay minerals. The other components are volcanic glass, plagioclase,

and trace amounts of phillipsite. Quartz and calcite can also be seen in the smear-slides.

X-ray diffraction of the bulk powdered material and oriented aggregates of the fine fraction (Figure 3) indicates that the clay minerals are primarily saponite, a trioctahedral Mg-smectite.

TEM photomicrographs of the fine fraction confirm that it is composed of small amounts of nontronite-type particles (Plate 1, figures 1 and 2) and more abundant well-crystallized saponites (Plate 1, figures 3, 4, and 5).

The common first diagenetic minerals in ashes, tuffs, and pyroclastic formations are zeolites, and the clay minerals (montmorillonites) are generally the result of later reaction (Iijima and Utada, 1966; Hay and Iijima, 1968; Sheppard and Gude, 1969; Surdam and Parker, 1972; Walton, 1975; Eaton, 1978; Hay, 1978). Therefore, the good preservation, size, and abundance of the clay particles point to a primary origin of the saponites. Zeolites, such as phillipsite, and nontronite are the secondary authigenic minerals from the alteration in marine environment of this volcaniclastic sequence. This mineral assemblage is common in marine-altered volcaniclastic material (Bonatti, 1972, Cronan, 1974).

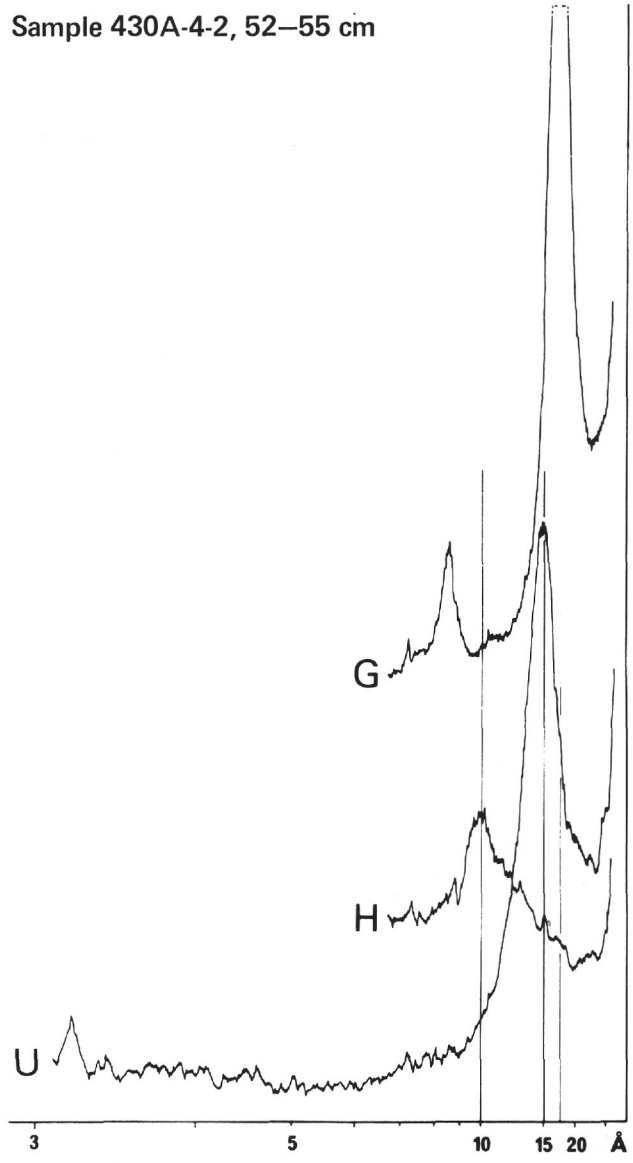

Figure 3. *X-ray diffraction chart on oriented aggregate of fine fraction (< 63 μm) of ash layer. U: untreated; G: ethylene-glycol-treated; H: heated.*

The Authigenic Clays in Yellow Aggregates from the Ferromanganese Sand, Site 431

The unconsolidated gravel from Site 431 contains 90 per cent iron-manganese crust fragments; the other components are firm, pale yellow or light yellowish-brown particles one to five millimeters in diameter. Some of these aggregates are stained by small spots of oxides or mixed with hard honey-brown slabs of phosphate. In order to determine the nature of these materials, investigations were made on very pure pale yellow clasts (Samples 431-1-1, 80–87 cm[b] and 431A-2-2, 52–54 cm).

X-ray diffraction data on non-oriented powder and oriented slides (Figure 4) show that the aggregates consist primarily of dioctahedral smectites with about 5 per cent phillipsite. The chemical analyses (Tables 2 and 3) confirm that the clays are Al–Fe smectites such as non-

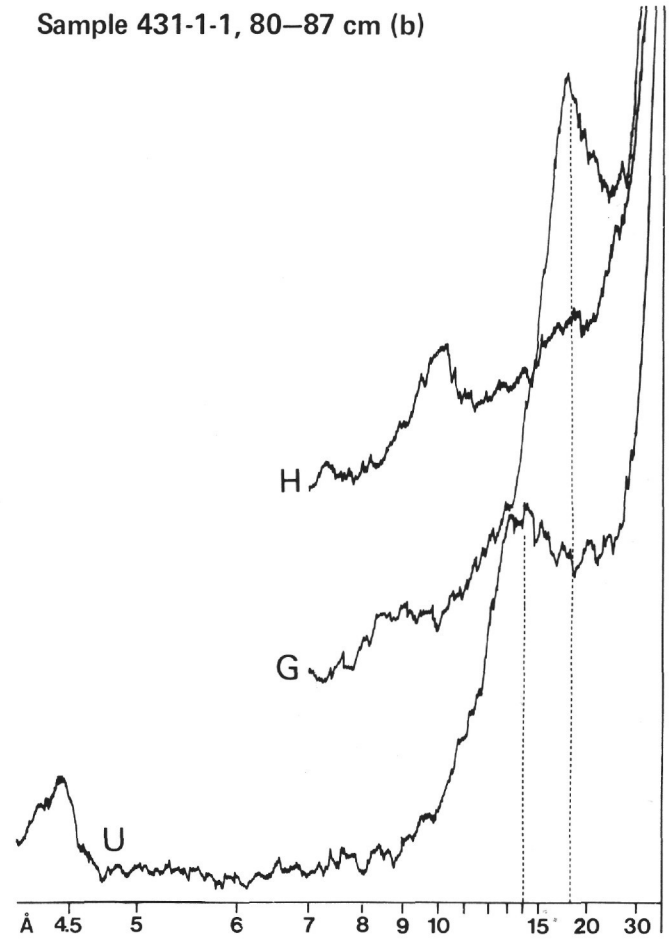

Figure 4. *X-ray diffraction chart of an oriented slide of the yellow firm particle. U: untreated; G: ethylene-glycol-treated; H: heated.*

TABLE 2
Chemistry of Sedimentary Samples, Sites 430, 432, 431: Major Elements (%)

Sample (Interval in cm)	SiO_2	Al_2O_3	MgO	CaO	Fe_2O_3	Mn_3O_4	TiO_2	Na_2O	K_2O	BaO	NiO	CO_2O_3	P_2O_5	Ign	Total
430-2-3, 43-52	25.4	9.2	2.58	9.2	14.9	12.2	1.94	2.04	1.76	–	0.40	–	–	12.82	92.44
2-4, 20-25	28.0	10.1	2.93	8.7	14.7	10.0	2.11	2.23	1.89	–	0.35	0.27	–	10.97	92.45
2,CC (oxide)	16.4	5.9	3.34	3.8	18.1	28.4	1.57	1.88	1.35	0.30	0.71	0.60	–	14.51	96.56
430A-1-1, 45-49	3.1	1.1	0.88	51.0	1.1	0.015	0.19	0.12	0.05	–	–	–	–	41.11	98.67
2-1, 127-129	9.6	2.5	1.29	44.5	3.2	0.065	0.58	0.22	0.09	–	–	–	–	36.68	98.72
2,CC	40.5	18.9	1.94	6.0	18.9	0.109	3.19	2.99	2.26	0.02	–	–	–	4.07	98.86
3,CC	9.1	2.6	1.16	45.0	3.0	0.048	0.53	0.17	0.09	–	–	–	–	37.74	99.44
4-1, 10-16	3.7	1.1	1.02	49.7	1.4	0.093	0.23	0.11	0.05	–	–	–	–	41.28	98.68
4-1, 64-66	47.4	14.0	7.03	3.9	15.4	0.108	2.57	3.82	2.38	–	0.11	–	–	3.53	100.25
4-2, 52-55	47.4	13.7	7.71	3.4	14.4	0.099	2.54	3.56	2.48	–	–	–	–	3.37	98.57
432-1-1, 30-34	6.4	1.6	0.84	48.4	1.7	0.032	0.19	0.06	0.05H	–	–	–	–	41.59	100.86
1-4, 76-80	41.5	8.9	3.63	9.9	19.0	0.053	1.26	1.93	2.72	–	–	–	–	11.63	100.67
431-1-1, 80-87(a)	3.3	1.0	2.32	3.9	15.4	43.9	1.04	0.06	0.05	0.38	1.11	0.97	–	23.12	96.55
1-1, 80-87(b)	51.5	14.7	4.23	1.6	12.1	0.094	1.63	3.52	4.07	0.12	0.1H	–	–	4.93	98.49
1-1, 80-87(c)	14.4	4.2	1.28	37.2	3.8	1.20	0.45	1.08	0.87	0.13	0.11	–	23.5	8.73	96.95
1*-1, 103-105	26.2	8.4	2.01	23.9	6.8	1.23	0.87	1.56	1.54	0.90	0.1H	–	14.5	8.02	95.93
431A-1-1, 138-140	30.0	6.7	3.08	6.5	10.7	21.7	0.68	2.05	1.41	0.66	0.36	0.38	–	11.63	95.85
2-1, 76-78	38.3	10.4	3.35	8.8	12.9	3.23	1.45	3.22	2.85	0.06	0.15	–	3.7	8.66	97.07
2-2, 43-45	7.1	1.1	2.12	3.4	18.3	40.8	0.92	1.87	0.71	0.53	0.44	0.42	–	15.99	93.70
2-2, 45-47(a)	3.3	0.7	2.09	4.4	15.3	44.4	1.18	1.11	0.52	0.26	0.66	–	–	16.05	89.97
2-2, 45-47(b)	32.3	9.4	3.54	1.9	12.5	16.1	1.40	2.03	2.04	0.20	0.54	–	–	10.80	92.75
2-2, 52-54	51.8	14.8	4.18	0.5	11.9	0.11	1.60	2.62	2.76	0.1H	0.1H	–	–	6.39	96.66

Note: Total iron is calculated as Fe_2O_3 and total manganese as Mn_3O_4. Ign is ignition loss at 1000°C. The sample descriptions are given in Table 1.

TABLE 3
Chemistry of Sedimentary Samples, Sites 430, 432, 431: Trace Elements (ppm)

Sample (Interval in cm)	Sr	Ba	V	Ni	Co	Cr	B	Zn	Ga	Cu	Pb	Sn
430-2-3, 43-45	462	2005	381	S	1300E	512	140	544	–	452	132	5H
2-4, 20-25	427	1844	414	S	S	626	98	361	–	450	125	5H
2,CC	689	2022	578	S	S	327	179	829	–	879E	145	5H
430A-1-1, 45-49	289	30	5	28	2H	34	17	25	2H	7	32	5H
2-1, 127-129	304	35	23	36	2H	52	17	53	2H	19	155	5H
2,CC	462	141	448	328	42	771	169	393	30	230	99	
3,CC	370	28	23	28	2H	68	17	39	2	25	31	5H
4-1, 10-16	382	18	11	16	2H	37	17	22	2H	9	35	6
4-1, 64-66	271	149	307	100	46	220	50	172	27	65	213	5H
4-2, 52-55	187	99	298	108	41	213	41	129	25	75	136	5H
432-1-1, 30-34	1239	233	5H	26	2H	55	40	33	2	9	10	15
1-4, 76-80	359	182	255	117	62	1143E	334	206	24	36	230	10
431-1-1, 80-87(a)	2568	3508	1600E	S	S	123	176	871	–	693E	375	14
1-1, 80-87(b)	114	656	50	355	3	196	374	281	21	278	307	5H
431A-1-1, 138-140	571	4108	376	S	S	90	131	515	–	340	147	5H
2-1, 76-78	131	265	96	S	232	161	263	159	28	189	129	5H
2-2, 43-45	887	3201	685	S	S	5	222	617	–	579E	1000E	5H
2-2, 52-54	30	59	49	161	17	220	318	241	19	133	272	5H

Note: H: value below the lower detection limit; S: value over the upper detection limit; E: extrapolated value; –: element not determined. For Samples 431-1-1, 80-87cm(c); 431-1*-1, 103-105cm; 431A-2-2, 45-47cm(a) and (b), trace-element data were not affected, because of the small quantity.

tronite or ferrous beidellite, with a total iron content about 12 per cent. The smectite particles are shown in the TEM photomicrograph of Plate 2, figure 5. The fine sheets are wind-edged. SEM photomicrographs bring out the structure and fabric of the clay aggregates (Plate 2, figures 1 to 4). They are similar to the montmorillonites shown by Borst and Keller (1969) and Bohor and Hugues (1971). The authigenic clayey particles initially formed as a result of successive depositions of 1-μm-thin layers (skins) of smectite around small smectite globules, giving rise to "onion-skin" textures. Finally, adjacent particles were included within the same layer, forming agglomerates.

The occurrence of iron smectite in present-day sediments in the vicinity of volcanic centers is known, and their authigenic origin has been demonstrated (Griffin

et al., 1968; Bonatti, 1972, Sayles and Bischoff, 1973; Aoki et al., 1974). In the sedimentary deposits of the Emperor Seamounts, the authigenic smectites differ from the detrital smectites as described above.

OTHER AUTHIGENIC COMPONENTS

Phosphates

Carbonate-apatite occurs in the upper part of the sedimentary deposits from Holes 430, 430A, 431, and 431A. It is generally associated with the authigenic clays with which it forms hard yellowish brown particles, and also fills cracks or slabs within the clay aggregates. The relationship between these components is established in the following part of this paper.

Since marine phosphorites were found by Murray and Renard (1891), their mineralogy, distribution, and origin have often been reviewed (Mero, 1965; Bromley, 1967; Tooms et al., 1969; Blatt et al., 1972; Bonatti, 1972; Christie, 1978). The most common hypotheses for the formation of marine phosphates is chemical precipitation from seawater, or re-emplacement of PO_4^{3-} units in pre-existing carbonates, in a relatively warm shallow-water environment with a low rate of detrital sedimentation. Marine phosphates occur on escarpments, banks, and the edges of continental shelves. Seamounts and guyots located far from continents may also provide an environment propitious for the formation of phosphates. Sheldon (1964) has shown that the latitudinal range of phosphorite deposition has been similar during geological time, between 5° and 40°, with a maximum at 23°.

Ferromanganese Oxihydroxides

Using the usual X-ray diffraction technique, we could not determine the mineral species or structure of the iron-manganese oxides. For the Leg 55 samples, then, the oxides are amorphous or most likely poorly crystalline todorokite. They are closely associated with clay, phosphate, and volcanic debris. The varying chemical composition of the Fe-Mn oxides has been established by microprobe analyses of polished samples, and is presented in the following section.

Marine authigenesis of iron-manganese oxihydroxides is well known. Since the Challenger Expedition (1873-1876), nodules and crusts have been described at varying depths and in a wide range of environments (Arrhenius, 1963; Mero, 1965; Cronan, 1974; Glasby, 1977, 1978). In shallow-water areas, manganese nodules are not uncommon (Price, 1967; Tooms et al., 1969), and their occurrence on seamounts has been described (Hamilton, 1956; Lonsdale et al., 1972; Cronan, 1977). Their occurrence on Suiko Seamount is discussed by Nohara and Nasu, 1977.

The most common hypothesis for the formation of ferromanganese oxides is the precipitation of Fe and Mn released in submarine volcanism or from seawater. The iron-manganese nodules and crusts are more frequent and more easily formed in oxidized cool deep water, in an oxidizing environment, and under volcanic influences.

CLASSIFICATION OF SEDIMENTARY DEPOSITS FROM ŌJIN, NINTOKU, AND YŌMEI SEAMOUNTS

On the basis of the mineralogical data, there are three major types of sedimentary materials on the Emperor chain: the primary volcanic material, biogenic calcareous phases, and authigenic minerals such as silicates (clays and scarce zeolites), phosphates, and metalliferous oxihydroxides. Variation in the percentage of these components is used to classify the sediments from Sites 430, 432, and 431 from the mostly detrital to predominantly authigenic (Table 4).

Geochemistry of the Sedimentary Deposits from Sites 430, 431, and 432

Methods

The geochemical data refer to the same set of samples studied above. Major- and trace-element analyses were performed following the method described by Besnus and Lucas (1970) and Besnus and Rouault (1973), using arc spectrometry and an ARL quantometer. The method consists of melting the sample in a mixture of lithium tetraborate and introducing the melt into a glycolated solvent. Trace elements were determined using graphite disks as described by Besnus and Lucas (1970). Na and K were determined by emission spectrometry. Relative precision is ±2 per cent for major elements and ±20 per cent for trace elements.

Results

Bulk chemical data are presented in Tables 2 and 3 for major (%) and trace (ppm) elements. Table 5 gives the principal element ratios. The compositions of sediments from Sites 430, 431, 432, and particularly the ferromanganiferous sequences are compared below with other marine ferromanganese deposits such as deep-sea nodules or hydrothermal formations.

Ternary Diagrams: Fe, Mn, and Transitional Elements

The characteristics of the ferromanganese deposits from Site 430 (Figure 5) are between those of the deep-sea nodules from the eastern equatorial Pacific, which are enriched in transitional elements, and the nodules from other Pacific seamounts and fossil concretions from Timor (Margolis et al., 1978). Hydrothermal

TABLE 4
Classification of the Sedimentary Deposits from Sites 430, 431, and 432, Emperor Seamounts

Environment and Influences	Sedimentary Deposits		Chronostratigraphy
Predominant detrital and volcanic influences	Ash layer	430A, Unit II	U. Paleocene
Detrital influence and reef environment	Calcareous volcanic sand	430A, Unit IB, base	U. Paleocene
Reef environment, biogenic influence dominant	Calcareous ooze	430A, Unit IB, top 432A, Unit II	U. Paleocene Paleocene
Predominant biogenic influence and pelagic environment	Foraminiferal oozes	432, Unit I 432, Unit III	Pleistocene Paleocene
Pelagic sedimentation, volcanic influence and authigenic process	Volcanic sands	432, Unit II 432A, Units I, III	Paleocene Paleocene
Authigenic process under volcanic influence and reef environment	Silty volcanic sands	430, Unit IA	Paleocene–Eocene
Dominant authigenic process	Ferromanganese sands	431 and 431A	Quaternary

TABLE 5
Ratios between Principal Elements of the Sedimentary Deposits, Sites 430, 432, and 431

Lithological and Mineralogical Facies	Sample (Interval in cm)	Si/Al	Mn/Fe	Fe/Ti	Ni/Mn	V/Fe
Altered basalt	430A-2,CC	1.88	0.006	5.9	4179	27.0
Volcanic ash	4-1, 64-66	2.98	0.007	6.9	1286	28.5
	4-2, 52-55	3.04	0.007	6.6	1515	29.6
Calcareous ooze	432-1-1, 30-34	3.52	0.019	10.4	1128	a
Calcareous volcanic deposits	430A-1-1, 45-49	2.48	0.014	6.7	2593	6.5
	2-1, 127-129	3.38	0.021	6.4	769	10.3
	3,CC	3.08	0.016	6.6	810	10.9
	4-1, 10-16	2.96	0.068	7.1	239	11.2
Authigenic clays	431-1-1, 80-87(b)	3.08	0.008	8.6	5245	5.9
	431A-2-2, 52-54	3.08	0.010	8.6	2033	5.9
Phosphates	431-1-1, 80-87(c)	3.02	0.325	9.8	1000	a
	1*-1, 103-105	2.74	0.186	9.1	a	a
	431A-2-1, 76-78	3.24	0.258	10.3	507	10.6
Carbonates, silicates, and oxides (calcareous ferromanganese gravel and mud)	430-2-3, 43-52	2.43	0.840	8.9	359	36.5
	2-4, 20-25	2.44	0.710	8.1	384	40.3
	431A-1-1, 138-140	3.94	2.089	18.2	181	50.2
	2-2, 45-47(b)	3.02	1.327	10.4	366	a
Ferromanganese oxides	430-2,CC	2.45	1.620	13.4	274	45.6
	431-1-1, 80-87(a)	2.90	2.940	17.2	276	148.0
	431A-2-2, 43-45	5.68	2.290	23.1	118	53.5
	2-2, 45-47(a)	4.15	2.989	15.0	162	a

[a]No values of trace-element contents.

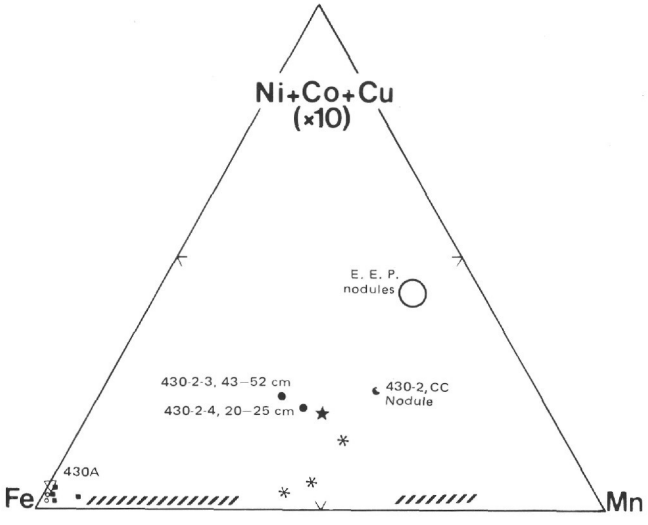

Figure 5. *Ternary diagram after Bonatti et al. (1972), Fe-Mn-(Ni + Co + Cu), showing the plots of Site 430 samples.*

- ● *Ferromanganese oxides (430).*
- ■ *Calcareous deposits (430A).*
- ○ *Ash layer samples (430A).*
- ∇ *Altered basalt pebble (430A).*
- * *Seamounts and Timor nodules (Margolis et al., 1978).*
- ★ *T 023 B Nodule from South Pacific (Hoffert et al., 1978[a]).*
- /// *Hydrothermal deposits from FAMOUS area (Hoffert et al., 1978[a]).*
- ○ *East Equatorial Pacific nodules (average).*

deposits (Hoffert, Perseil, et al., 1978) are poor in transitional elements. The oxides of the sediments from Ōjin seamount are close to those from the South Pacific formed in a volcanic environment (Hoffert, Karpoff, et al., 1978).

At Site 431, iron-manganese oxihydroxides making up the abundant crust fragments are similar to the nodule from Site 430 (Figure 6), but are more enriched in manganese than in transition elements.

It appears that the Emperor Seamount concretions were formed under volcanic influence. They have composition intermediate between the deep-sea concretions and seamount nodules. The chemical features of the authigenic oxides from the Emperor Seamounts indicate that depth is not a restrictive condition for enrichment in transition elements and trace elements. The predominant influences seem to be the physicochemical characteristics of environment, such as oxygenation, alteration of the volcaniclastic material, and a low rate of sedimentation.

Inter-Element Relationships

The relations between Mn/Fe and Ni/Mn ratios (Table 5; Figures 7 and 8) for all sediments samples establish the following: (1) Primary silicates have high iron and nickel contents, (2) Though the authigenic oxides contain high percentages of nickel, they do not concentrate it as much as the authigenic clays, (3) Calcareous and phosphatic facies have low nickel and manganese contents.

Chromium, copper, zinc, cobalt, and lead behave similarly to nickel. Relative to manganese, they are less enriched than nickel in the oxides, and stay highly concentrated within the volcanic minerals. Cronan (1977) established a negative correlation between cobalt concentration and depth. The Co contents of the Leg 55 concretions are in accordance with the depths of the seamounts.

The titanium contents of oxides and crusts are lower than the average given by Cronan (1977) for the Pacific

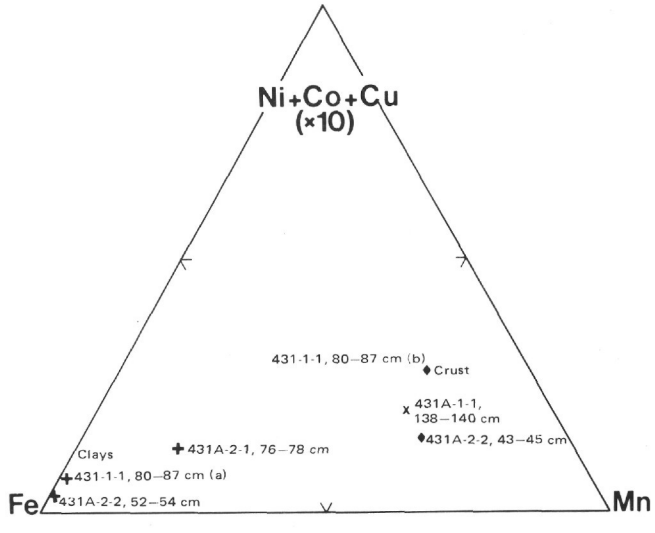

Figure 6. *Ternary diagram Fe-Mn-(Ni + Co + Cu), with the data for the Site 431 samples.*

- ♦ *Ferromanganese crust fragments.*
- \+ *Clays and phosphates.*
- × *Bulk sedimentary deposits (crust and clays).*

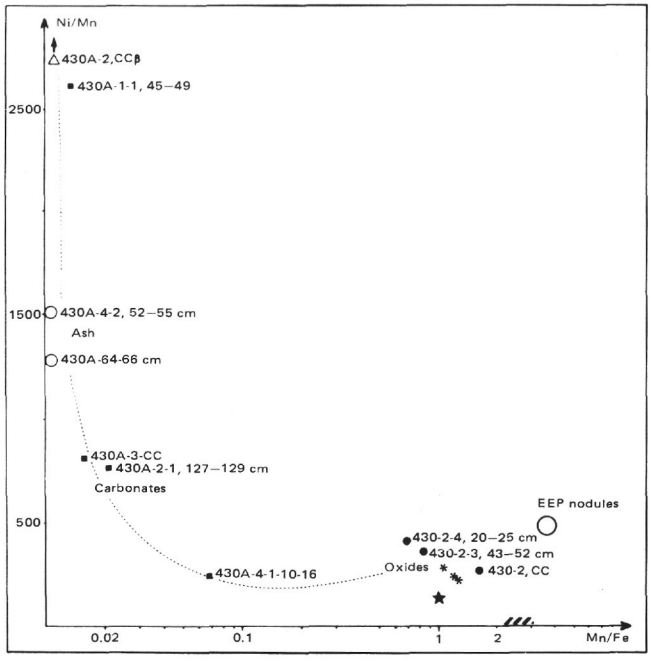

Figure 7. *Relation between nickel-to-manganese ratio and manganese-to-iron ratio in sedimentary deposits of Site 430. Data from total analyses (Tables 2 and 3); same symbols as in Figure 5.*

* *Seamounts and Timor nodules.*

/// *Hydrothermal deposits.*

★ *T 023 B South Pacific nodule.*

○ *EEP: average for east equatorial Pacific nodules. Logarithmic scale for Mn/Fe ratio.*

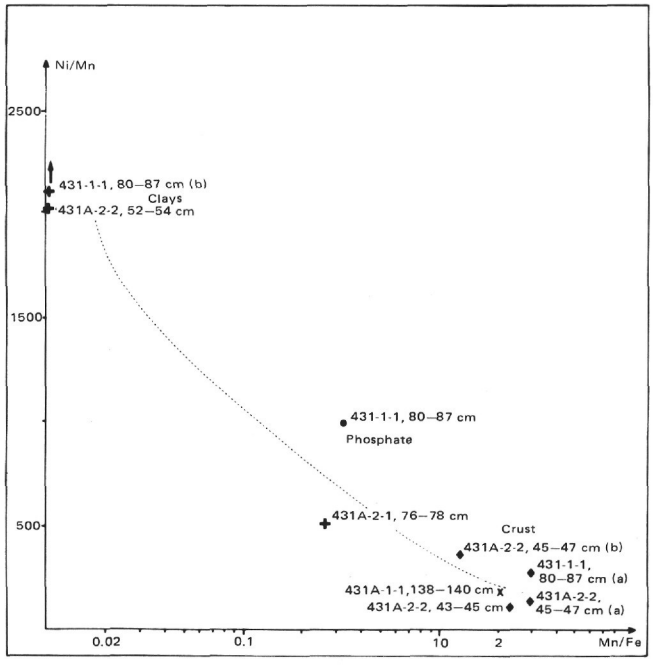

Figure 8. *Relation between nickel-to-manganese ratio and manganese-to-iron ratio in sedimentary deposits of Site 431. Same symbols as in Figure 6. Logarithmic scale for Mn/Fe ratio.*

seamounts. In the detrital and authigenic silicates, titanium content is well correlated with aluminum content.

The association of vanadium with iron is well known. Primary clays from the ash layer are distinct from authigenic clays by virtue of their high V/Fe ratio (Table 5 and Figure 9). The vanadium leached from the volcanic material precipitates preferentially into the authigenic oxides and phosphates.

Primary clays from the ash layer and the authigenic smectites differ in their iron and magnesium contents. The smectites have a higher iron content, and the ash saponites are rich in magnesium. The occurrence of authigenic smectites is also characterized by increasing boron contents (Landergreen and Carjaval, 1969; Walker, 1972).

Calcium–Strontium Relations

The third prevalent component of the Leg 55 sediments is calcareous, and is composed of foraminiferal nannofossil ooze and reef deposits. These sediments are poor in all trace elements other than strontium and lead. The correlation diagram of calcium versus strontium (Figure 10) shows that the foraminifer oozes from Site 432 have a normal Sr/Ca ratio (Turekian, 1964). Diagenetic evolution of reef calcareous deposits induces impoverishment in strontium, such as that described for the lagoonal formation at Site 433 (Karpoff, this volume).

The Sr/Ca ratio is constant in the basalt, residual volcanic silicates, and authigenic compounds. From basalt to authigenic smectites, strontium and calcium both decrease. In the ferromanganese oxides, they increase.

Summary

Factors affecting distribution of the elements in the mineral phases of the heterogeneous deposits from the Emperor Seamounts are predominantly hydrolysis of the volcanic material, differential solubility of the various elements in seawater, and their precipitation in the authigenic compounds. Our hypothesis for the origin of the elements is halmyrolysis of detrital volcaniclastic material. This hypothesis is common, but more often concerns alteration of the products from submarine vulcanism (Bonatti and Nayadu, 1965; Arrhenius and Bonatti, 1965; Cronan, 1974).

Microscopic Investigations and Microprobe Analyses

Methods

Microscopic chemical analyses have been performed by X-ray dispersive energy spectroscopy (SEM Cameca 07 and TRACOR System) with an accelerating voltage of 20 kv and sample current of about 0.2 nA. Count time was 100 seconds. Since all the analyses took place under the same conditions, a comparison of the semiquantitative results is possible. Maps of the distribution of the principal elements in particular zones of the samples are discussed in what follows.

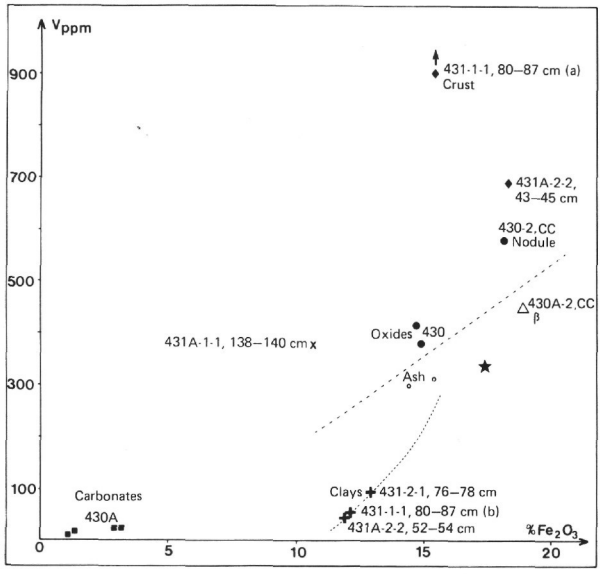

Figure 9. *Correlation between Fe_2O_3 (%) and V (ppm) contents in sedimentary deposits from Sites 430 and 431. Same symbols as in Figures 5 and 6.*

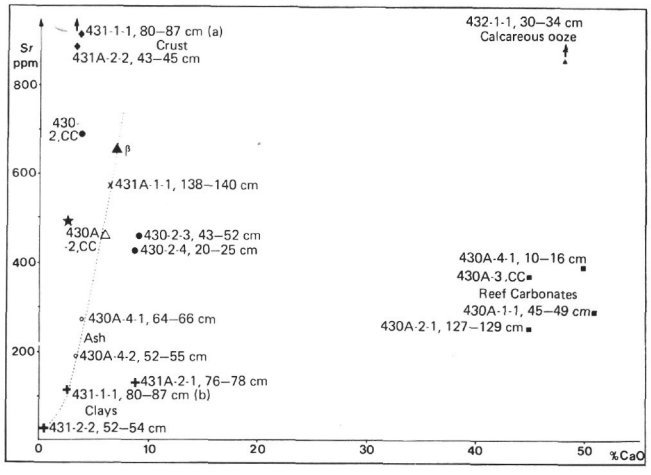

Figure 10. *Relation between Sr (ppm) and Cao (%) contents of sedimentary deposits from Sites 430, 431, and 432. Same symbols as in Figure 10.*

★ *T 023 B South Pacific nodule (Hoffert et al., 1978[b]).*

▲ *Basalt: average of contents from Hole 430A Flow Unit 1.*

Nodule from Hole 430

A small rounded nodule, about two centimeters in size, was found in the core catcher sample of Core 2, Hole 430. The SEM investigations define its structure and the chemical variations of the successive ferromanganese layers.

The nucleus or "core", oblong in shape, is pale brown and yellow. It is composed of plagioclase, zeolites, and small amounts of clay. Magnetite or ilmenorutile also occurs. These minerals are well intermingled and coated ((Figure 11; Plate 3; Plate 4, figure 2). Spectrochemical data indicate that the plagioclase is rich in calcium and sodium, the zeolites contain potassium (phillipsite), and the clays are iron-rich. The distribution maps of the prevalent elements are given in Plate 3. Occurrence of small amounts of quartz and calcite is established.

Thus, the major part of the nodule core is detrital sedimentary material, coated and cemented by authigenic clays, and blades of zeolite.

The cortex of the nodule consists of successive concentric layers (Plate 4), as follows, from inside to outside:

Layer C_1: A massive, regular, fine lamina and completely surrounding the nucleus.

C_2: A lightly disturbed massive layer, composed of two sublayers, C_2a and C_2b, separated by a very thin nickel-rich lamina (Plate 4, figures 3 and 5). The C_2 layer is discontinuous around the core.

NiL: This layer appears pale gray on the photomicrographs. It is characterized by very high contents of manganese and nickel; it does not contain iron. This nickeliferous layer is discontinuous and irregular around the nucleus (Plate 4, figures 3, 5, and 6).

C_3: This layer encircles completely the core and comprises two sublayers. The inner has an irregular colloform laminated structure; the outer band contains phosphate grains, small volcanic debris, and siliceous remains like the nodule core components. These particles are darker on the SEM photomicrographs, but appear white or pale gray in polished section.

C_4: The outermost oxide deposits comprise three units. The first, C_4a is predominantly massive with mottled zones; C_4b is massive and contains several conic columnar zones. Inside the oxide laminae of such conic structures, the lower sides of cracks are fringed by very thin pale gray deposits (Plate 4, figure 4). This manganese deposit has a very high concentration of nickel similar to the NiL layer. The outermost C_4c band is heterogeneous and mottled, and contains siliceous or phosphatic fragments.

The successive layers have cracks and clefts coated by iron-manganese oxides or small amounts of siliceous material.

The internal layered structure of the nodule is common, and was described by Sorem (1967) and Sorem and Fewkes (1977).

The chemical variations of the layers were established by spectroscopic measurements made under constant conditions, as described above. Measurements made across the nodule layering give the results presented in Figures 12 and 13.

The relation between the Mn/Fe and Mn/Ni ratios brings out the occurrence of five types of oxides: manganese-nickel oxide without iron (1); iron-manganese oxide without nickel (5), and three intermediate types of oxides with correlative changes of the Mn/Fe and Mn/Ni ratios (2, 3, 4). Therefore, nickel occurs preferentially within the manganese-rich oxide more than the oxide rich in iron. In the intermediate types of iron-manganese oxide, the calcium content decreases while

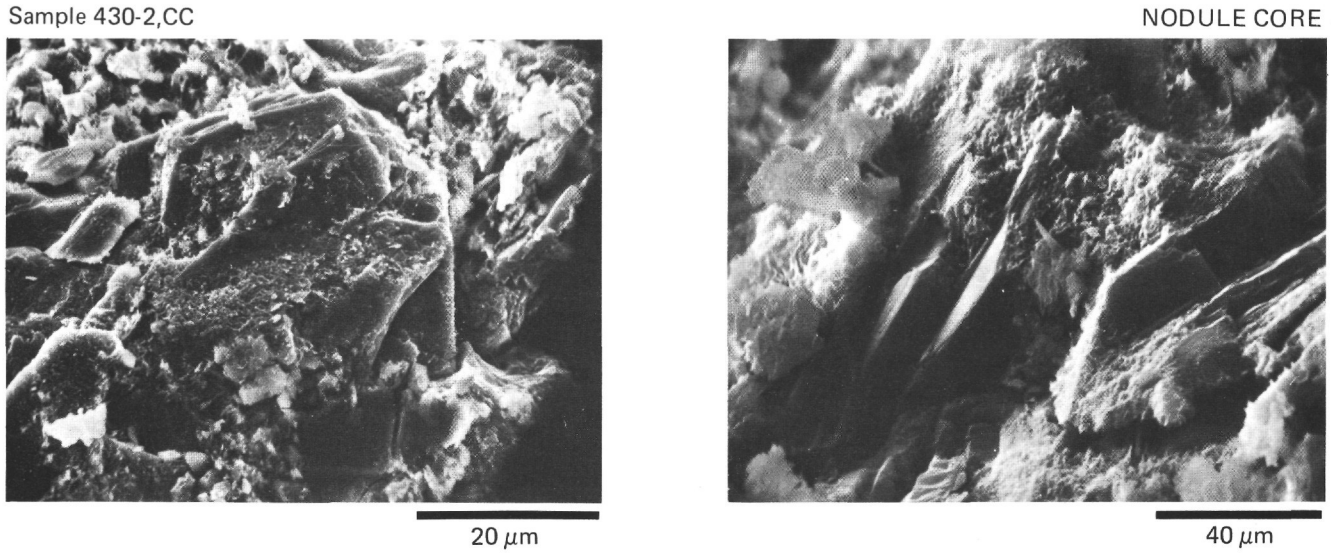

Figure 11. *SEM photomicrographs of the nodule core made up of plagioclases with fine clay deposits here and there (Sample 430-2,CC).*

the nickel content increases. The manganese oxide rich in nickel also contains copper and small amounts of aluminum, magnesium, and potassium. The iron oxides have high contents of silicon, calcium, and titanium, and small amounts of sodium. Some cracks crossing the layers contain clays with high magnesium and iron contents.

The distribution of the five different oxides is independent of the layer ordering. The variation of the Mn/Ni ratio from the innermost layer to the outermost layer, presented in Figure 13, shows that the change is not progressive and regular from layer to layer. Nevertheless, iron seems to be higher and nickel depleted outward from the center e.g., C_2a, C_2b, C_4b). The nickeliferous laminae show sharp contacts with the adjacent laminae, and their nickel content is drastically higher than that of these adjacent laminae. The cortex average content of nickel oxide is 0.71 per cent (Table 2). Supposing that the thin nickeliferous laminae make up about 10 per cent of the cortex, the concentration of nickel would be about 7 to 10 per cent in these layers. Sorem and Fewkes (1977) have determined that the layers rich in Mn, Ni, K, and Cu are well crystallized as compared with the amorphous layers rich in iron. They indicate that the crystalline material is todorokite and birnessite.

Thus, deposition of the different types of oxides was not gradual and continuous. During some periods, the physicochemical properties of the environment induced formation of well-crystallized, nickel-rich manganese oxides. The marked changes in the oxides can be produced by varying reducing-oxidizing conditions, as by alternate periods of submarine sedimentation or scour (Sorem, 1967; Cheney and Vredenburgh, 1968). Nohara and Nasu (1977) proposed that Quaternary glacial influenced the periodic patterns of elements in manganese nodules from Suiko Seamount.

Ferromanganese Crust Fragment

The sedimentary deposits from Site 431 are predominantly iron-manganese crust fragments and sands. In the lower part of lithologic Unit II, we have sampled a crust fragment (Sample 431A-2-2, 45–47 cm) three centimenters thick which comprises two zones: a black massive iron-manganese band, and a breccia-like heterogeneous part composed of volcanic remains, siliceous authigenic fragments, and a first generation of micronodules coated with iron-manganese oxides.

Plate 5 shows the polished section of this crust fragment. The two zones are very distinct; the SEM photomicrographs, by secondary electrons and backscattered electrons (Plate 5, figures 1 and 2), establish structural and chemical characteristics of the two parts. In the backscattered-electron picture, the oxides rich in manganese appear clearer than the iron-rich oxides; the siliceous particles, such as the clays filling up a crack, are darker.

The outer zone has a columnar structure in places chaotic and mottled. Well-crystallized quartz occurs between the curved laminae (Plate 5, figures 3 and 5). Small crystals of zeolites occur within the cracks with the clay fillings (Plate 5, figures 3 and 4). Authigenesis of zeolites strongly associated with iron-manganese oxides in concretions has been described, but generally the crystals are bigger (Sorem and Fewkes, 1977; Burns and Burns, 1978). Occurrences of authigenic microcrystalline silica have been observed in other crusts and nodules (Karpoff, 1977; Hoffert, Karpoff, et al., 1978).

Microprobe analyses and distribution maps of prevalent elements, made on an area located between the two

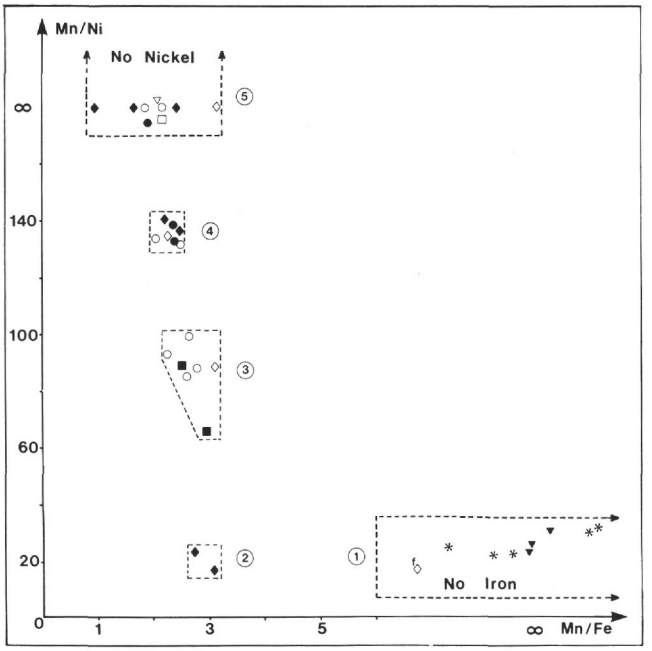

Figure 12. *Relation between Mn/Fe ratio and Mn/Ni ratio in the cortex layers of nodule from Site 430 (X-ray dispersive-energy spectroscopy coupled to SEM, semiquantitative analyses). Five types of oxihydroxides have been determined.*

- ● *C_1 layer.*
- ○ *C_2 layers.*
- ▼ *C_3 layers.*
- ▽ *C_4 layers.*
- ♦ *C_4 conical structure.*
- ◇ *C_4 outermost layer.*
- ■ *First layer before C_1 which joins core and cortex (innermost layer).*
- □ *Cross-oxides in cracks.*
- * *Nickel-rich layers between C_2a–C_2b layers and C_2b–C_3 layers.*

zones described above (Plate 6), establish the occurrence of different oxides as in the oxides layers of the nodule from Site 430.

The breccia-like zone contains manganese oxides, rich in nickel, which are in places crystal-shaped, filling some vacant site in the primary mineral. These oxides contain small amounts of copper. The mixed oxides (Ni–Mn–Fe) are scarce. Micronodules are iron-rich and mixed with clays. Well-preserved volcanic feldspars occur. The particles are coated with oxides rich in iron. In the same area (Plate 5, figures 1 and 2), the volcanic debris and minerals are fringed by thin laminae of clays and iron–titanium oxides.

The columnar crust zone comprises intermediate iron–manganese oxides relatively uniform in composition (Mn, Fe, Ca, Ti, Si). The colloform features of these concretions have been interpreted as stromatolithic structures (Jenkins, 1977; Schaaf et al., 1977).

Firm Sediment Aggregate

The iron–ferromanganese sand from Site 431 contains yellow firm particles composed of authigenic smectites. Microprobe analyses and distribution maps of elements were performed using a polished section of a yellowish brown aggregate stained by black iron–manganese oxides and crossed by a crack fringed with oxides and filled with phosphates and clays (Figure 14). The analyzed area brings out the successive stages of authigenic deposits, shown in Plate 7:

1) The first authigenic smectites have high iron contents (B).

2) The clays are coated with phosphates (A) in thin laminae or fillings of interstices.

3) The oxides fringe the crack; in the first deposit (C), iron and titanium prevail; the second deposit (D) is a manganese oxide rich in nickel, and contains trace amounts of calcium and magnesium; the third layer (E) is an iron-manganese oxide containing small amounts of calcium and titanium.

4) At the end, the crack is coated with clays (F) which have higher potassium and lower calcium contents than the first authigenic smectites. Small silicate particles rich in potassium, such as phillipsite, are enclosed (G).

Summary

Scanning-electron microscope and microscope data indicate successive stages of authigenic compounds formation, as follows:

1) The volcaniclastic remains are cemented by clays and scarce zeolites (e.g., nodule nucleus).

2) Authigenic clays start to form small firm particles (e.g., pale yellow aggregates).

3) Particles are cemented with phosphates (e.g., yellowish brown aggregates).

4) Aggregates are coated with iron–manganese oxides; the deposits varying in chemical composition are formed during alternate periods. The first deposits are enriched in titanium; some layers are rich in manganese and nickel.

5) A reworking period induces the formation of unconsolidated remains of latter authigenic phases, subsequently cemented by iron–manganese oxides (e.g., breccia zone of crust fragment and C_4b layer of nodule).

6) Subsequently, the aggregates are coated again with iron–manganese oxides structurally and chemically distinct from the former oxides (e.g., upper colloform zone of the crust fragment, last band of the nodule).

7) The last authigenic compounds are zeolites, clays, and microcrystalline silica.

CONCLUSION

The sedimentary deposits on the Emperor Seamounts, and particularly on Ōjin and Yōmei seamounts, are volcanigenic sediments. They are composed of residual detrital fragments and a variety of authigenic mineral phases. The halmyrolysis of volcanic material induces the formation of successive authigenic com-

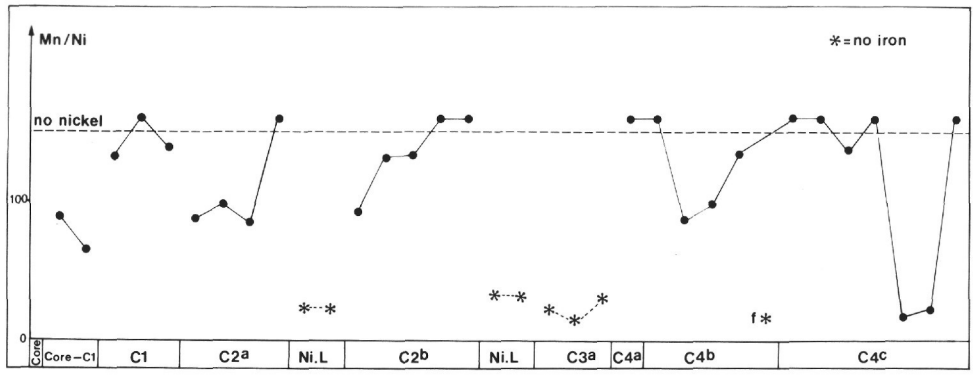

Figure 13. *Variation of the Mn/Ni ratio in the cortex of nodule from Site 430, innermost layers to outermost layers. The symbol * indicates the nickel-rich layers. (SEM with X-ray dispersive-energy spectroscopy data).*

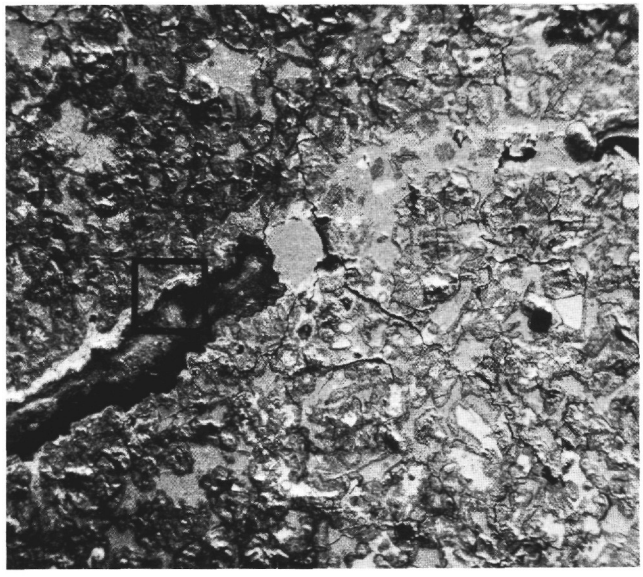

Figure 14. *SEM photomicrograph (by backscattered electrons) of polished section from sedimentary aggregate (Sample 431-2-1, 103–105 cm). Location of the zone studies in Plate 7;* × *30.*

pounds: silicates, phosphates, and iron-manganese oxides. The successive changes in the nature and composition of the authigenic phases appear to result from varying depositional environments.

The beginning of alteration of volcaniclastic material induces the authigenesis of smectites during a period of low sedimentation rate.

The phosphate deposits occur preferentially in shallow warm water during periods of non-sedimentation. Phosphates derive from sea water, but some hydrothermal contribution cannot be excluded (Froelich et al., 1977). According to the hypothesis of Sheldon (1964), Yōmei Seamount would have been situated below 35°N during the phosphate deposit period, probably during the Eocene–Pleistocene hiatus.

The deposition of iron-manganese oxides is easier in a cooler, deeper, and oxidized environment. Small changes in the oxidizing–reducing conditions, temperature, and volcanic influences such as steam and rates of alteration of the detrital basalt material, induce formation of varying iron-manganese-nickel oxides.

The permanent high-energy environment during the last period strongly reworked the deposits. The volcanosedimentary deposits did not result in the formation of a continuous indurated crust as described by Morgenstein (1967) and Hoffert, Karpoff, et al. (1978). The sandy facies was maintained.

The volcanigenic deposits from Yōmei Seamount differ from those found on Suiko Seamount (particularly with reference to the volcanic sand overlying the reef deposits [Karpoff, this volume]) by the occurrence of abundant iron-manganese concretions. The characteristics of these concretions are intermediate between those from typical seamount nodules and volcanigenic deep-sea nodules and crusts. The position of Site 431 on a lateral faulted terrace increases the influences of the open sea. The volcanic activity seems to have been constant during the subsidence of the seamount.

For Nintoku Seamount, the drill site is located on top of a reef flat, and this situation can explain the lack of volcanigenic sediments like those from Yōmei Seamount and the deposition of pelagic sediments overlying basalt and reef deposits.

The sedimentary sequence from Ōjin Seamount appears to contain typical reef and pelagic deposits and volcanigenic iron-manganese formations intermediate between the other two types.

ACKNOWLEDGMENTS

The analytical work was performed with the technical support of the Centre de Sédimentologie et Géochimie de la Surface of the C.N.R.S. and the Instituts de Géologie et de Minéralogie, Strasbourg. The authors are grateful to André Schaaf and Norbert Clauer for suggestions, and to M. Gruner for helpful photographic work. The TEM observations were made with Denise Trauth.

REFERENCES

Aoki, S., Kohyama, N., and Sudo, T., 1974. An iron-rich montmorillonite in a sediment core from the northeastern Pacific, *Deep Sea Research*, v. 21, pp. 865–875.

Arrhenius, G., 1963. Pelagic sediments. *In* Hill, M. N. (Ed.), *The Sea:* New York (Interscience), v. 3, pp. 655–718.

Arrhenius, G. and Bonatti, E., 1965. Neptunism and volcanism in the ocean, *Progress in Oceanography*, Sears Ed., v. 3, pp. 7-22.

Besnus, Y. and Lucas, J., 1970. Méthode de dosage de 18 éléments majeurs et traces dans les roches sédimentaires et les produits d'altération par spectrométrie à lecture directe. *Coll. Nat. C.N.R.S.*, 923, pp. 93-106.

Besnus, Y. and Rouault, R., 1973. Une méthode d'analyse des roches au spectromètre d'arc à lecture directe par un dispositif d'electrode rotative, *Analusis*, v. 2, pp. 111-116.

Blatt, H., Middleton, G., and Murray, R., 1972. *Origin of sedimentary rocks*: Englewood Cliffs, N. J. (Prentice-Hall Inc.), p. 634.

Bohor, B. F. and Hughes, R. E., 1971. Scanning electron microscopy of clays and clay minerals, *Clays and Clay Min.*, v. 19, pp. 49-54.

Bonatti, E., 1972. Marine authigenesis of minerals. *In* Fairbridge, R. W. (Ed.), *Encycl. Geochim. Envir. Sci.*, v. IVA, pp. 48-56.

Bonatti, E., Kraemer, T., and Rydell, H. S., 1972. Classification and genesis of submarine iron-manganese deposits. In *Ferromanganese Deposits on the Ocean Floor*. Lamont-Doherty Geological Observatory of Columbia University, Palisades, N. Y., pp. 149-166.

Bonatti, E. and Nayadu, Y. R., 1965. The origin of manganese nodules on the ocean floor, *Am. Jour. of Sci.*, v. 263, pp. 17-39.

Borst, R. L. and Keller, W. D., 1969. Scanning electron microphotographs of API reference clay minerals and other selected samples, *Proc. Int. Clay Conf., Tokyo*, v. 1, pp. 871-901.

Bromley, R. G., 1967. Marine phosphorites as depth indicators, *Mar. Geol.*, v. 5, pp. 503-509.

Burns, V. M. and Burns, R. G., 1978. Diagenetic features observed inside deep-sea manganese nodules from the north equatorial Pacific, *Scanning Electron Microscopy*, v. 1, pp. 245-252.

Cheney, E. S. and Vredenburgh, L. D., 1968. The role of iron sulfides in the diagenetic formation of ion-poor manganese nodules, *Jour. Sedim. Petrol.*, v. 38, pp. 1363-1365.

Christie, R. L., 1978. Sedimentary phosphate deposits—An interim review, *Geol. Surv. Canada Pap.*, v. 78, p. 20.

Cronan, D. S., 1974. Authigenic minerals in deep-sea sediments. *In* Hill, M. N. (Ed.), *The Sea:* New York (Interscience), v. 5, pp. 491-525.

_____, 1977. Deep-sea manganese nodules: distribution and geochemistry. *In* Glasby, G. P. (Ed.), *Marine Manganese Deposits:* Elsevier Scientific Publishing Co., v. 15, pp. 11-44.

Eaton, G. P., 1978. Volcanic ash deposits. *In* Fairbridge, R. W., and Bourgeois, J. (Ed.), *The Encyclopedia of Sedimentology,* v. VI, pp. 843-850.

Elderfield, H., 1977. The form of manganese and iron in marine sediments. *In* Glasby, G. P. (Ed.), *Marine manganese deposits:* Elsevier Scientific Publishing Co., v. 15, pp. 269-289.

Froelich, P. N., Bender, M. L., and Heath, G. R., 1977. Phosphorous accumulation rates in metalliferous sediments on the East Pacific Rise, *Earth Planetary Sc. Letters*, v. 34, pp. 351-359.

Glasby, G. P., 1977. Marine manganese deposits, *Elsevier Oceanography Series:* Elsevier Scientific Publishing Co., v. 15, p. 523.

_____, 1978. Deep sea manganese nodules in the stratigraphic record: evidence from DSDP cores, *Marine Geol.*, v. 28, pp. 51-64.

Griffin, J. J., Windom, H., and Goldberg, E. D., 1968. The distribution of clay minerals in the world ocean, *Deep-Sea Research*, v. 15, pp. 433-459.

Hamilton, E. L., 1956. Sunken islands of the Mid-Pacific mountains, *Mem. Geol. Soc. Am.*, v. 64, p. 97.

Hay, R. L., 1978. Volcanic ash diagenesis. *In* Fairbridge, R. W., and Bourgeois, J. (Ed.), *The Encyclopedia of Sedimentology:* v. VI, pp. 850-851.

Hay, R. L. and Iijima, A., 1968. Nature and origin of palagonite tuffs of the Honolulu group on Oahu, Hawaii, *Mem. Geol. Soc. Am.*, v. 116, pp. 331-376.

Hoffert, M., Karpoff, A. M., Clauer, N., Schaaf, A., Courtois, C., and Pautot, G., 1978. Néoformations et altérations dans trois faciès volcanosédimentaires du Pacifique Sud, *Oceanol. Acta*, v. 1, pp. 187-202.

Hoffert, M., Perseil, E. A., Hekinian, R., Choukroune, P., Needham, H. D., Francheteau, J., and Le Pichon, X., 1978. Hydrothermal deposits sampled by diving saucer in Transform Fault "A" near 37°N on the Mid-Atlantic Ridge, Famous area, *Oceanol. Acta*, v. 1, pp. 73-86.

Iijima, A. and Utada, M., 1966. Zeolites in sedimentary rocks, with reference to the depositional environments and zonal distribution, *Sedimentology*, v. 7, pp. 327-357.

Jenkyns, H. C., 1977. Fossil nodules. *In* Glasby, G. P. (Ed.), *Marine Manganese Deposits:* Elsevier Scientific Publishing Co., v. 15, pp. 87-108.

Karpoff, A. M., 1977. Plättchenformiges silizium mit ploymetallischen konkretionen vergesellschaftet aus den rezenten sedimenten des Nördlischen Pazific. In *Ergebnisse der Manganknollen-Wissenschafts fahrt VA.13-2*, Bundesanstalt für Geowissenschaften und Rohstoffe, Hannover, p. 1.

Landergreen, S. and Carjaval, M. C., 1969. Contribution to the geochemistry of boron—III: The relationship between boron concentration in marine clay sediments and the salinity of depositional environment expressed as adsorption isotherm, *Arkiv. Mineral. Geol.*, v. 5, pp. 11-22.

Lonsdale, P., Normark, W. R., and Newman, W. A., 1972. Sedimentation and erosion on Horizon Guyot, *Geol. Soc. Am. Bull.*, v. 83, pp. 289-316.

Margolis, S. V., Ku, L. T., Glasby, G. P., Fein, C. D., Audley-Charles, M. G., 1978. Fossil manganese nodule from Timor: geochemical and radiochemical evidence for deep-sea origin, *Chem. Geol.*, v. 21, pp. 185-198.

Mero, J. L., 1965. The mineral resources of the sea, *Elsevier Oceanography Series:* Elsevier Scientific Publishing Co., v. 1, p. 312.

Mise au Point Collective, 1975. Techniques de preparation des mineraux argileux en vue de l'analyse par diffraction des Rayons-X, *Notes Tech. Inst. Géol.*, U. L. P., Strasbourg, v. 1, p. 21.

Morgenstein, M., 1967. Authigenic cementation of scoriaceous deep-sea sediments west of the Society Ridge, South Pacific, *Sedimentology*, v. 9, p. 105-118.

Murray, J. and Renard, A. F., 1891. Deep-sea deposits, *Rep. Sci. Results of Voyage* H. M. S. Challenger. Edinburgh (Neil and Co.), p. 525.

Nohara, M. and Nasu, N., 1977. Mineralogical and geochemical characteristics of manganese nodules from the Suiko Seamount, Northwestern Pacific Ocean. 2: Geochemical aspect and its origin, *Bull. Geol. Sur. Japan*, v. 28-9, pp. 615-622.

Price, N. B., 1967. Some geochemical observations on manganese-iron oxide nodules from different depth environments, *Marine Geol.*, v. 5, pp. 511-538.

———, 1976. Diagenesis in marine sediments. *In* Riley, J. P., and Chester, R. (Ed.), *Chemical Oceanography:* London (Academic Press), v. 6, pp. 1–58.

Sayles, F. L., and Bischoff, J. L., 1973. Ferromanganoan sediments in the equatorial east Pacific, *Earth and Planetary Sc. Letters*, v. 19, pp. 330–336.

Schaff, A., Hoffert, M., Karpoff, A. M., and Wirrmann, D., 1977. Association de structures stromatolithiques et de foraminifères sessiles dans un encroûtement ferromanganésifère à coeur granitique en provenance de l'Atlantique nord, *C. R. Acad. Sc.*, Paris, v. 284-D, pp. 1705–1708.

Sheldon, R. P., 1964. Paleolatitudinal and paleogeographic distribution of phosphorites, *U. S. Geol. Surv. Prof. Paper*, v. 501-C, pp. 106–113.

Sheppard, R. A., and Gude, A. J., 1969. Diagenesis of tuffs in the Barstow Formation, Mud Hills, San Berdanino County, Arizona, *U. S. Geol. Surv. Prof. Paper*, v. 634, p. 35.

Sorem, R. K., 1967. Manganese nodules: nature and significance of internal structure, *Econ. Geology*, v. 62, pp. 141–147.

Sorem, R. K. and Fewkes, R. H., 1977. Internal characteristics. *In* Glasby, G. P. (Ed.), *Marine Manganese Deposits:* Elsevier Scientific Publishing Co., v. 15, pp. 147–184.

Surdam, R. C. and Parker, R. D., 1972. Authigenic aluminosilicate mineral in the tuffaceous rocks of the Green River Formation, Wyoming, *Geol. Soc. Am. Bull.*, v. 83, pp. 689–700.

Tooms, J. S., Summerhayes, C. P., and Cronan, D. S., 1969. Geochemistry of marine phosphorites and manganese deposits, *Oceanogr. Mar. Biol. Annu. Rev.*, v. 7, pp. 49–100.

Turekian, K. K., 1964. The marine geochemistry of strontium, *Geochim. Cosmochim. Acta*, v. 28, p. 1479–1496.

Trauth, D., Ehret, G., Eberhart, J. P., and Weber, F., 1977. Microscopie électronique et minéraux argileux: résultats obtenus et orientations actuelles, *Notes Tech. Inst. Géol.*, U. L. P., Strasbourg, v. 7, p. 16.

Walker, C. T., 1972. Boron geochemistry in marine environment. *In* Fairbridge, R. W. (Ed.), *The Encyclopedia of Geochemistry and Environmental Sciences:* New York (Van Nostrand Reinhold), v. IVA, pp. 90–92.

Walton, A. W., 1975. Zeolitic diagenesis in Oligocene volcanic sediments, Trans-Pecos, Texas, *Geol. Soc. Am. Bull.*, v. 86, pp. 615–624.

PLATE 1

Electron microscope studies on ash layer fine fraction
(<63 μm, Sample 430A-4-2, 52–55 cm).

Figure 1 — General view of the clay fraction composed of smectites.

Figure 2 — Laths of saponite.

Figure 3 — Nontronite particles.

Figure 4 — High magnification of one saponite lath.

Figure 5 — Diffraction diagram made on the saponite monocrystal of figure 4.

PLATE 1

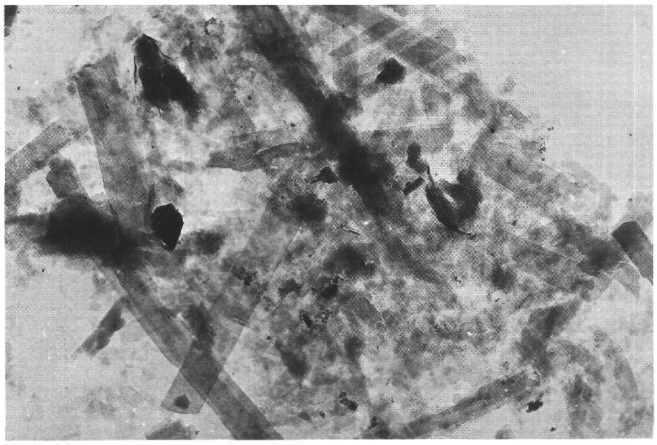

1

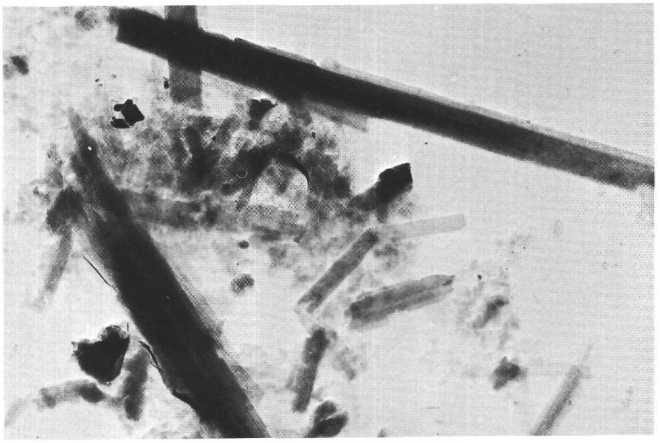

2

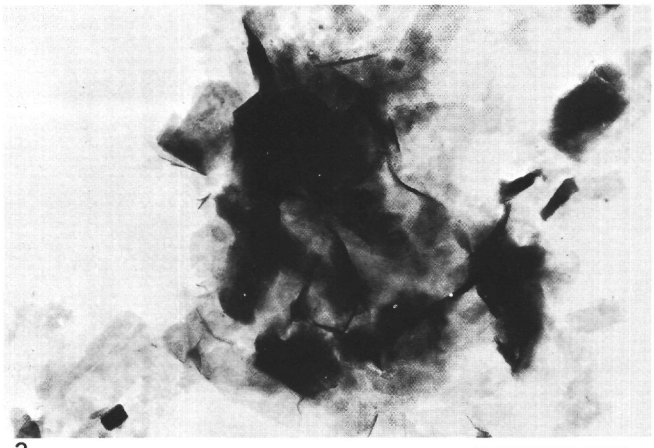

3

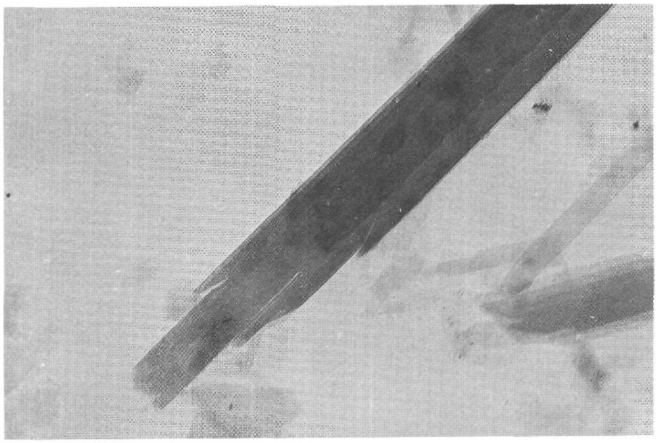

4

5

PLATE 2
Electron photomicrographs of yellow clay aggregates
in the ferromanganiferous sand at Site 431
(Sample 431-1-1, 80–87 cm[b], bulk sample).

Figure 1 S.E.M. general view, showing the spherical structures of the smectite mass and globules with successive deposits of smectites.

Figure 2 Detail of a globule.

Figure 3 In section, the mass and globules have the same aspect.

Figure 4 High magnification of the surface and core of a globule; the mass is fringed by vermiculated fine deposits of smectites.

Figure 5 T.E.M. photomicrograph of the smectites.

PLATE 2

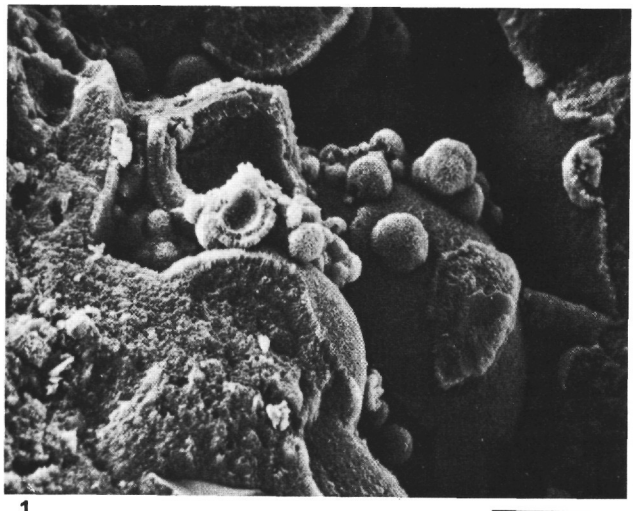

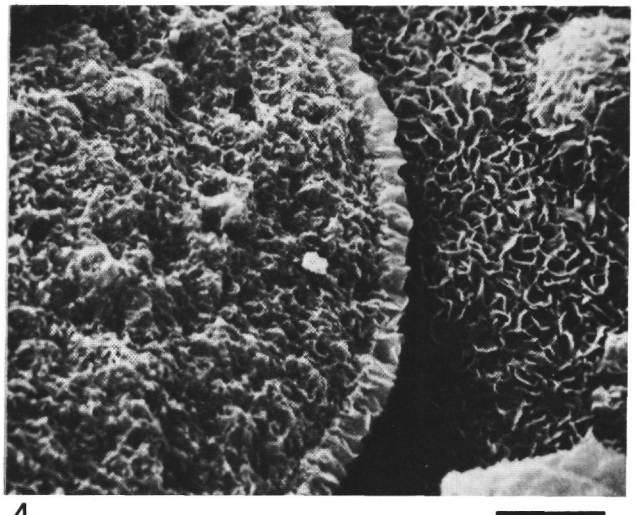

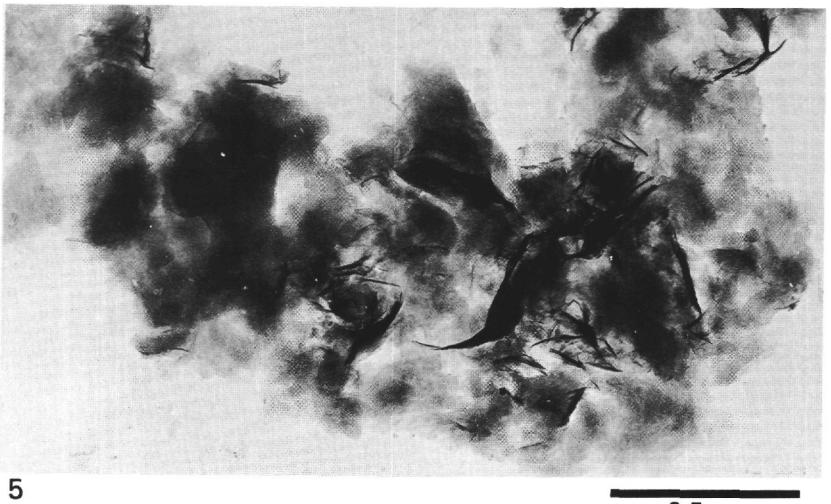

PLATE 3

S.E.M. chemical studies of nodule core (Sample 430-2, CC).
Repartition of Ca, Si, Fe, K, Na, and Ti.

a: Ca–Na silicates (plagioclases), and between crystals: Ca-carbonate clays, and K-zeolites.

b: Iron–titanium oxides.

c: Small quartz fragments.

d: Cavities.

PLATE 3

Sample 430-2,CC
NODULE CORE

40 μm

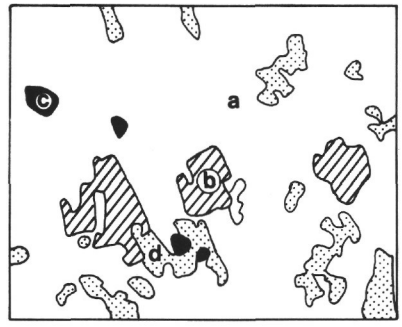

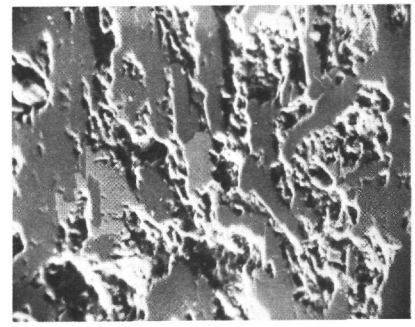

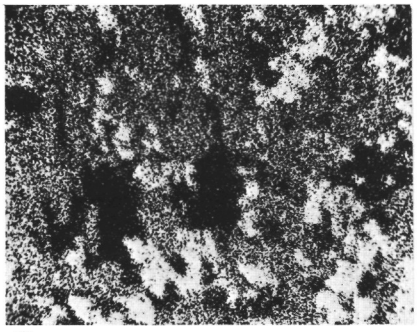
Ca

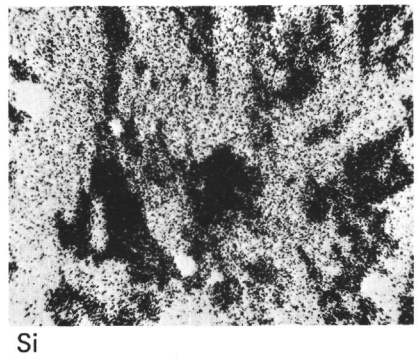
Si

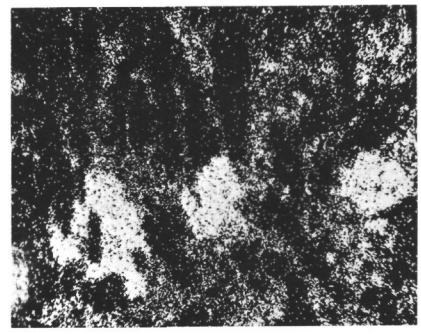
Fe

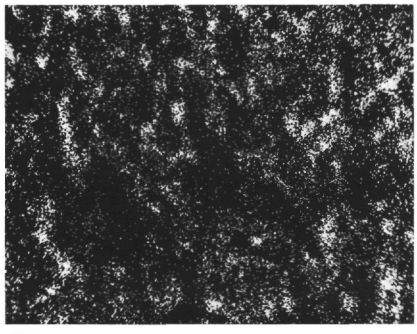
K

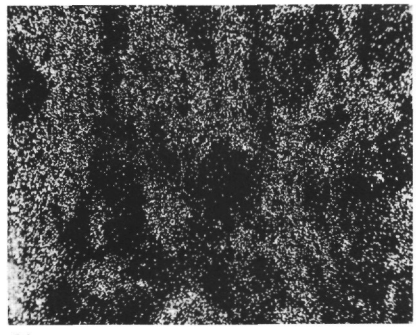
Na

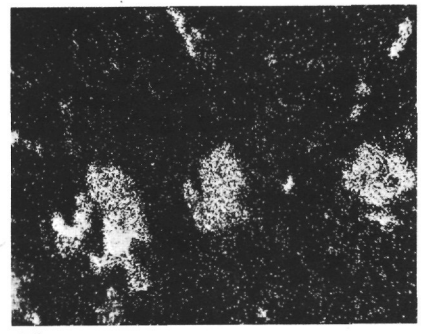
Ti

PLATE 4
General view of polished section of nodule from
Site 430 (Sample 430-2, CC).

Figure 1 (Central photographs): structure of nodule with oblong siliceous core, and four principal iron-manganese layers making up the cortex.

Around the central view, higher magnification of particular zones:

Figure 2 Detail of Ca-Na silicates (plagioclases) which make up the core mass and small spots of K-rich silicate (phillipsite ?).

Figure 3 Detail of the structure of the cortex for the three innermost iron-manganese layers. The second layer (C_2a-C_2b and Ni layer) is not continuous around the core.

Figure 4 Detail of the conical structure of the C_4b layer. The crack is fringed, on the innermost side only, by a fine deposit of clear nickel-manganese oxide.

Figure 5 Higher magnification of the three innermost layers.

Figure 6 Detail of the nickel-manganese layer (Ni-L) which marks the limit between layer 2 and layer 3— Equivalent repartition map of nickel.

PLATE 4

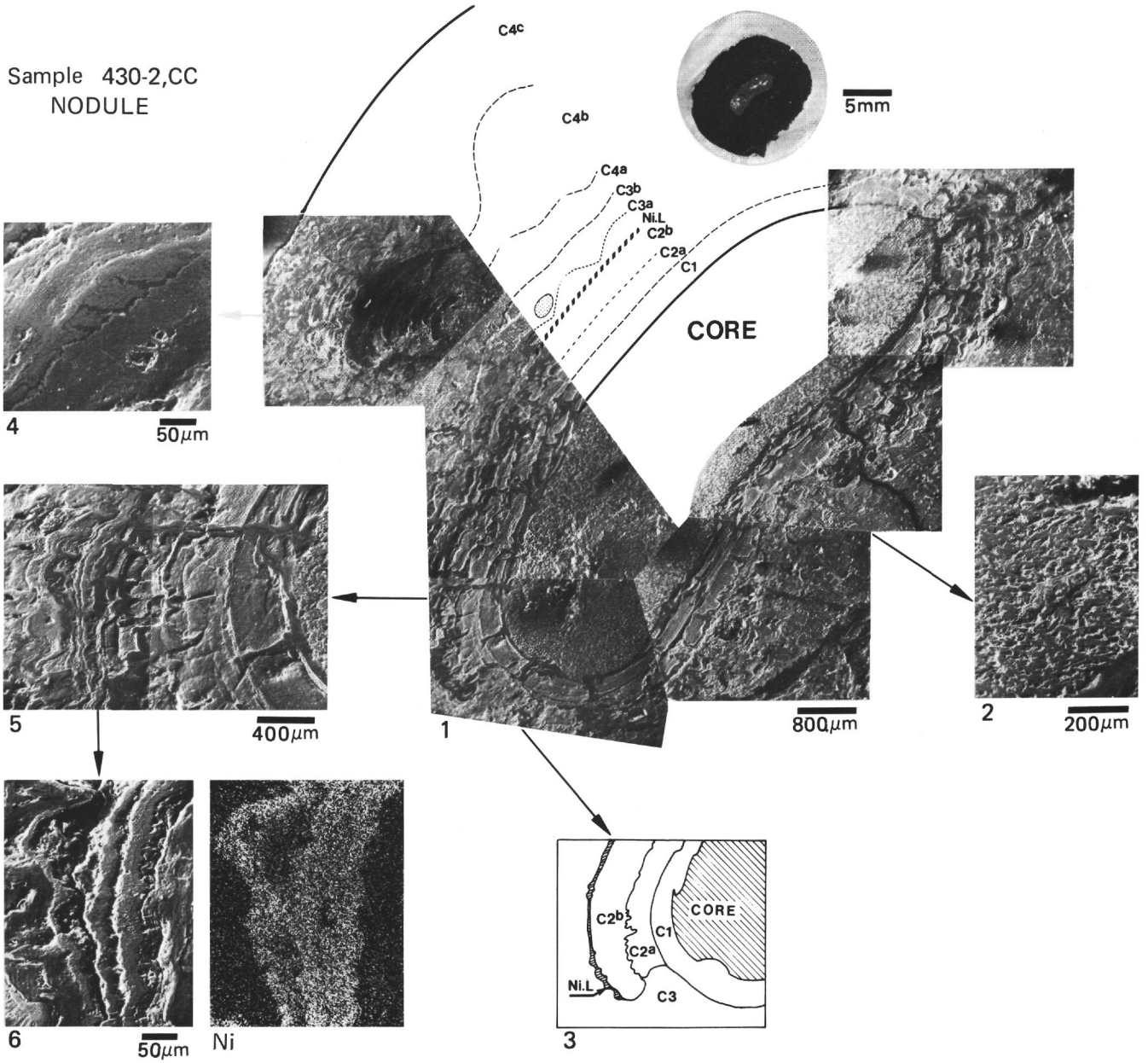
Sample 430-2,CC
NODULE
C4c
C4b
C4a
C3b
C3a
Ni.L
C2b
C2a
C1
CORE
5mm
4
50μm
5
400μm
1
800μm
2
200μm
6
50μm
Ni
3
C2b
C1
CORE
C2a
Ni.L
C3

PLATE 5

S.E.M. investigations on a polished section of a crust fragment from sedimentary deposits of Site 431 (Sample 431A-2-2, 45–47 cm). This crust is composed of two zones: the upper zone is iron-manganese oxides with "puffs of pipe" structures. The lower part has a breccia-like structure containing fragments of clays, calcium phosphate, and a first generation of micronodules, enclosed in a second generation of iron-manganese oxides.

Figure 1 S.E.M. photomicrographs of the limit between the two zones, (secondary electrons picture, inclined plane). Schematic drawing above.

Figure 2 Same zone as figure 1, but by backscattered electrons; the manganese-rich oxides appear very light; iron-manganese oxides are pale gray, silicate minerals are dark-gray.

Figure 3 High-magnification of the cleft zone and boundary between crust and breccia.

Figure 4 Detail of small zeolitic crystals growing on the side of the cleft crust zone (upper square on the schematic drawing).

Figure 5 Small authigenic quartz crystals in the fine layers of crust "cusps" (lower square on the schematic drawing).

Note: On the drawing, the zone worked on Plate 6 is shown by broken-line square.

PLATE 5

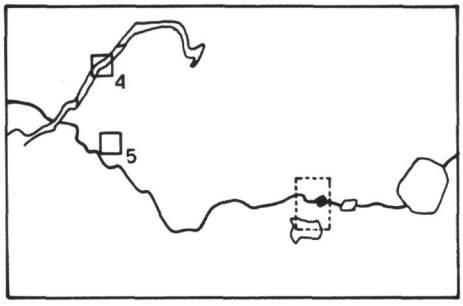

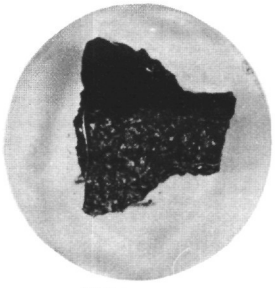

Sample 431A-2-2, 45–47cm
CRUST FRAGMENT

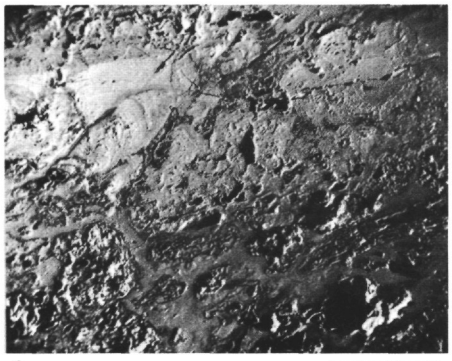

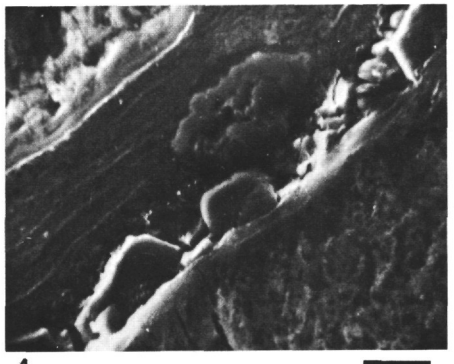

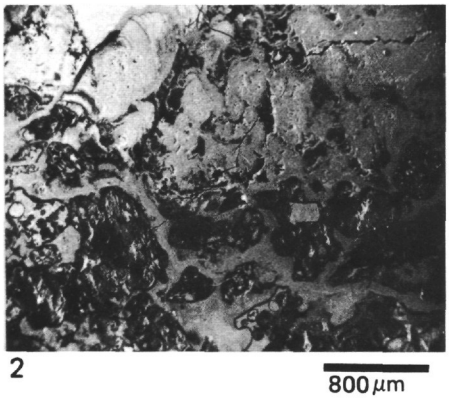

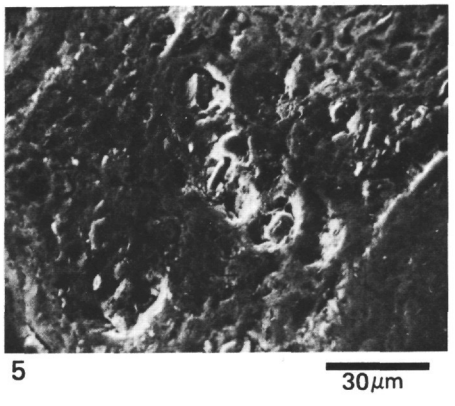

PLATE 6

S.E.M. spectrometry studies on crust fragment (Sample 431A-2-2, 45–47 cm), at the boundary between crust and breccia facies (see Plate 5 for location on the polished section).

Breccia zone: a: Mn–Ni-rich oxide; a*: Mn–Fe–Ni oxide; b: Fe-rich oxide; c: Fe–Mn oxide; d: K-silicate (feldspar).

Crust zone: c*: Fe–Mn oxide.

PLATE 6

Sample 431A-2-2, 45–47cm
CRUST FRAGMENT

100μm

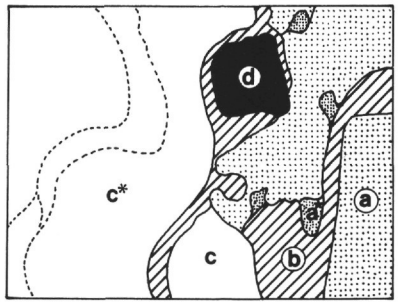

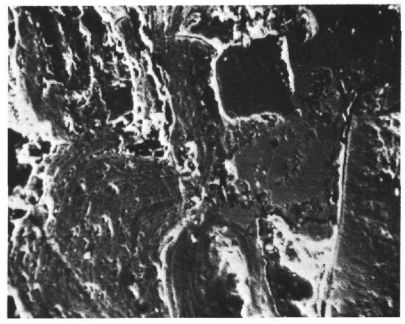

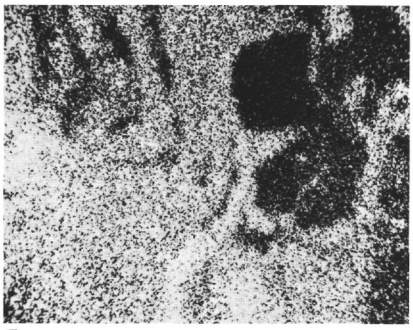

Fe

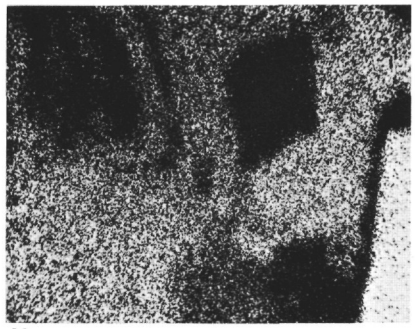

Mn

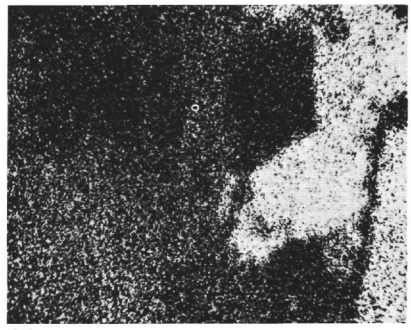

Ni

PLATE 7

S.E.M. spectrometry studies on a zone of the firm sedimentary clast (Sample 431-1-1, 103–105 cm; see Figure 14 for location on the polished section).

Distribution maps of Al, Si, Ca, Mg, Fe, Ti, K, and Ni

A: carbonate-apatite (high Ca-content zone).

B: Fe–Mg smectites with trace amounts of Ti.

C: Fe–Ti oxide, first deposit.

D: Mn–Ni oxide with trace amounts of Ca and Mg, second deposit.

E: Fe–Mn oxide with trace amounts of Ti, third deposit.

F: Fe–K clays within the crack. In this area very small crystals of barite occur.

G: K-silicates, probably zeolites.

PLATE 7

Sample 431-1-1, 103–105cm
SEDIMENT CLAST

100μm

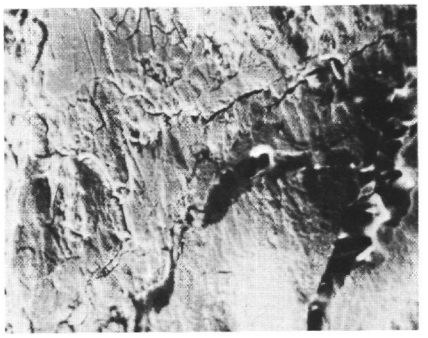

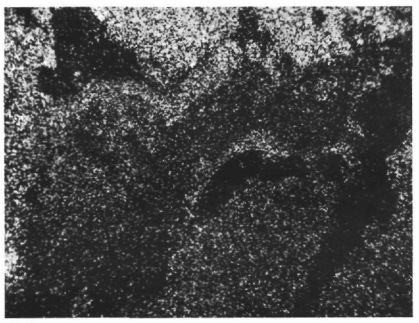
Al

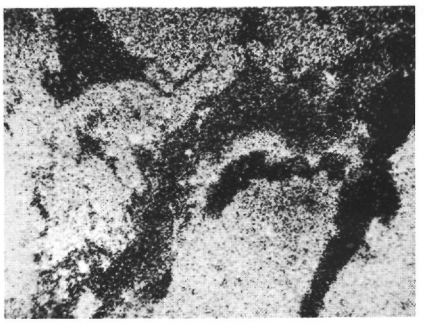
Si

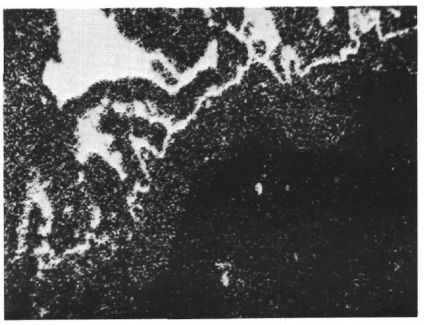
Ca

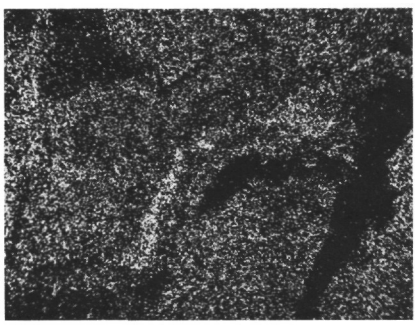
Mg

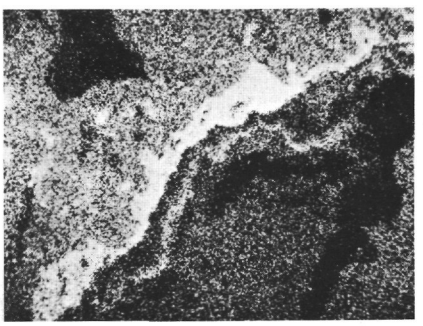
Fe

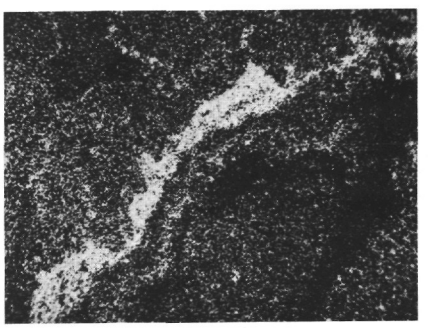
Ti

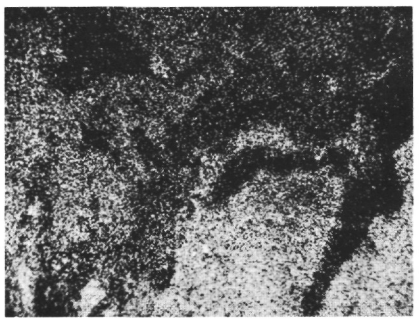
K


Mn

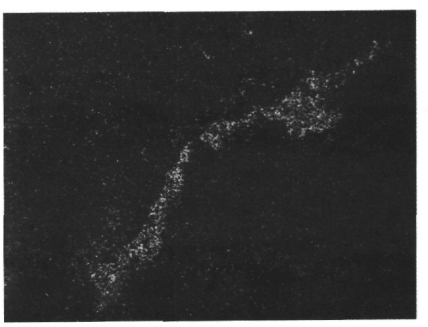
Ni